



# UNIVERSITÀ DI PARMA

## ARCHIVIO DELLA RICERCA

University of Parma Research Repository

A space-time Energetic BIE method  
for 3D Elastodynamics. The Dirichlet case.

This is the peer reviewed version of the following article:

*Original*

A space-time Energetic BIE method  
for 3D Elastodynamics. The Dirichlet case / Aimi, A.; Dallospedale, S.; Desiderio, L.; Guardasoni, C.. - In:  
COMPUTATIONAL MECHANICS. - ISSN 0178-7675. - 72:5(2023), pp. 885-905. [10.1007/s00466-023-02312-  
z]

*Availability:*

This version is available at: 11381/2940311 since: 2024-10-11T08:38:20Z

*Publisher:*

Springer

*Published*

DOI:10.1007/s00466-023-02312-z

*Terms of use:*

Anyone can freely access the full text of works made available as "Open Access". Works made available

*Publisher copyright*

note finali coverpage

(Article begins on next page)

Dear Author,

Here are the proofs of your article.

- You can submit your corrections **online**, via **e-mail** or by **fax**.
- For **online** submission please insert your corrections in the online correction form. Always indicate the line number to which the correction refers.
- You can also insert your corrections in the proof PDF and **email** the annotated PDF.
- For fax submission, please ensure that your corrections are clearly legible. Use a fine black pen and write the correction in the margin, not too close to the edge of the page.
- Remember to note the **journal title**, **article number**, and **your name** when sending your response via e-mail or fax.
- **Check** the metadata sheet to make sure that the header information, especially author names and the corresponding affiliations are correctly shown.
- **Check** the questions that may have arisen during copy editing and insert your answers/ corrections.
- **Check** that the text is complete and that all figures, tables and their legends are included. Also check the accuracy of special characters, equations, and electronic supplementary material if applicable. If necessary refer to the *Edited manuscript*.
- The publication of inaccurate data such as dosages and units can have serious consequences. Please take particular care that all such details are correct.
- Please **do not** make changes that involve only matters of style. We have generally introduced forms that follow the journal's style. Substantial changes in content, e.g., new results, corrected values, title and authorship are not allowed without the approval of the responsible editor. In such a case, please contact the Editorial Office and return his/her consent together with the proof.
- If we do not receive your corrections **within 48 hours**, we will send you a reminder.
- Your article will be published **Online First** approximately one week after receipt of your corrected proofs. This is the **official first publication** citable with the DOI. **Further changes are, therefore, not possible.**
- The **printed version** will follow in a forthcoming issue.

#### **Please note**

After online publication, subscribers (personal/institutional) to this journal will have access to the complete article via the DOI using the URL: [http://dx.doi.org/\[DOI\]](http://dx.doi.org/[DOI]).

If you would like to know when your article has been published online, take advantage of our free alert service. For registration and further information go to: <http://www.link.springer.com>.

Due to the electronic nature of the procedure, the manuscript and the original figures will only be returned to you on special request. When you return your corrections, please inform us if you would like to have these documents returned.

# Metadata of the article that will be visualized in OnlineFirst

---

ArticleTitle	A space–time energetic BIE method for 3D elastodynamics: the Dirichlet case	
--------------	---	--

---

Article Sub-Title		
-------------------	--	--

---

Article CopyRight	The Author(s), under exclusive licence to Springer-Verlag GmbH Germany, part of Springer Nature (This will be the copyright line in the final PDF)	
-------------------	---	--

---

Journal Name	Computational Mechanics	
--------------	-------------------------	--

---

Corresponding Author	FamilyName	<b>Desiderio</b>
	Particle	
	Given Name	<b>L.</b>
	Suffix	
	Division	Department of Mathematical, Physical and Computer Sciences
	Organization	University of Parma
	Address	Parma, Italy
	Phone	
	Fax	
	Email	luca.desiderio@unipr.it
	ORCID	<a href="http://orcid.org/0000-0002-3924-0939">http://orcid.org/0000-0002-3924-0939</a>

---

Author	FamilyName	<b>Aimi</b>
	Particle	
	Given Name	<b>A.</b>
	Suffix	
	Division	Department of Mathematical, Physical and Computer Sciences
	Organization	University of Parma
	Address	Parma, Italy
	Phone	
	Fax	
	Email	
	ORCID	

---

Author	FamilyName	<b>Dallospedale</b>
	Particle	
	Given Name	<b>S.</b>
	Suffix	
	Division	Department of Sciences and Methods for Engineering
	Organization	University of Modena
	Address	Modena, Italy
	Phone	
	Fax	
	Email	
	ORCID	

---

Author	FamilyName	<b>Guardasoni</b>
	Particle	
	Given Name	<b>C.</b>
	Suffix	
	Division	Department of Mathematical, Physical and Computer Sciences
	Organization	University of Parma
	Address	Parma, Italy
	Phone	
	Fax	
	Email	
	ORCID	

---

---

Schedule	Received	26 Oct 2022
	Revised	
	Accepted	1 Mar 2023

---

Abstract	<p>We consider the retarded potential boundary integral equation, arising from the 3D elastic (vector) wave equation problem, endowed with a Dirichlet condition on the boundary and null initial conditions. For its numerical solution, we employ a weak formulation related to the energy of the system and we discretize it by a Galerkin-type boundary element method (BEM). This approach, called energetic BEM, has been already applied in the context of time-domain acoustic (scalar) wave propagation and it has revealed accurate and stable even on large time intervals of analysis. In particular, when standard (constant) shape functions for time discretization are employed, the double integration in time can be performed analytically. Then, one is left with the task of evaluating double space integrals, whose integration domains are generally delimited by the wave fronts of the primary and the secondary waves. Since the accurate computation of the integrals involved in the numerical scheme is a key issue for the stability of the method, we propose an efficient evaluation strategy, based on the exact detection of the integration domain. The presented numerical tests show the effectiveness of the proposed approach.</p>
----------	--

---

Keywords (separated by '-')	3D elastodynamics - Space-time boundary integral equations - Energetic boundary element method
-----------------------------	--

---

Footnote Information	A. Aimi, L. Desiderio and C. Guardasoni: Members of the INdAM-GNCS Research Group, Italy.
----------------------	---

---



# A space–time energetic BIE method for 3D elastodynamics: the Dirichlet case

A. Aimi<sup>1</sup> · S. Dallospedale<sup>2</sup> · L. Desiderio<sup>1</sup> · C. Guardasoni<sup>1</sup>

Received: 26 October 2022 / Accepted: 1 March 2023

© The Author(s), under exclusive licence to Springer-Verlag GmbH Germany, part of Springer Nature 2023

## Abstract

We consider the retarded potential boundary integral equation, arising from the 3D elastic (vector) wave equation problem, endowed with a Dirichlet condition on the boundary and null initial conditions. For its numerical solution, we employ a weak formulation related to the energy of the system and we discretize it by a Galerkin-type boundary element method (BEM). This approach, called energetic BEM, has been already applied in the context of time-domain acoustic (scalar) wave propagation and it has revealed accurate and stable even on large time intervals of analysis. In particular, when standard (constant) shape functions for time discretization are employed, the double integration in time can be performed analytically. Then, one is left with the task of evaluating double space integrals, whose integration domains are generally delimited by the wave fronts of the primary and the secondary waves. Since the accurate computation of the integrals involved in the numerical scheme is a key issue for the stability of the method, we propose an efficient evaluation strategy, based on the exact detection of the integration domain. The presented numerical tests show the effectiveness of the proposed approach.

**Keywords** 3D elastodynamics · Space–time boundary integral equations · Energetic boundary element method

## 1 Introduction

The design of a suitable, efficient and accurate numerical method to solve elastodynamic problems is encountered in many academic and industrial applications. To cite a few examples: the development of a powerful forward engine in the framework of Full-Waveform Inversion (FWI) for the estimation of the elastic parameters in the underground; the study of fluid–structure interactions; the numerical solution of contact problems. Even if different directions exist, the use of a boundary integral equation (BIE) technique, whose discretization is known as the boundary element method (BEM), is an appealing choice because it allows to handle problems defined on the exterior of bounded domains as easily as those defined in the interior, without the introduction of an artificial

boundary to truncate the computational domain. Furthermore, this technique requires the discretization only of the domain boundaries, leading to a drastic reduction of the total number of degrees of freedom of the problem. To simulate elastic wave propagation, most BEMs assume time invariant harmonic excitation so that the unknowns are time invariant complex fields. Even if this analysis has been used for many years by engineers, the transient behaviour witnessed in the real world may only be recovered by calculation of many frequency-domain models and inverse discrete Fourier transform. Unfortunately, solving one frequency-domain BEM equation in a 3D domain is computationally very costly, since the resulting linear system is fully-populated, so that acceleration techniques have to be employed in order to obtain accurate solutions in reasonable computational times. Most of them are based on the compression of the system matrix aiming at applying efficient direct or iterative solvers (see e.g. hierarchical matrices [9, 16, 19] and fast multiple methods [35]).

An alternative is to drop the time invariant assumption and formulate the transient problems in the time-domain, which is usually called Time-Domain BEMs (TD-BEMs). As well summarized in [24, 30], the discretization of TD-BIEs by collocation methods has some advantages in implementation

A. Aimi, L. Desiderio and C. Guardasoni: Members of the INdAM-GNCS Research Group, Italy.

✉ L. Desiderio  
luca.desiderio@unipr.it

<sup>1</sup> Department of Mathematical, Physical and Computer Sciences, University of Parma, Parma, Italy

<sup>2</sup> Department of Sciences and Methods for Engineering, University of Modena, Modena, Italy

due to its simplicity but gives rise to instability issues (see e.g. [23, 34]), avoided by some variational approaches as well as by convolution quadrature methods [27], but these latter with some drawbacks highlighted in [13].

Among the variational approaches, as the one theoretically analyzed in the milestone paper [14], a Galerkin TD-BEM for the discretization of the BIEs related to acoustic (scalar) wave propagation problems has been introduced in [2]. The proposed technique is based on a natural energy identity satisfied by the solution of the corresponding differential problem, which leads to a space–time weak formulation of the BIEs with precise continuity and coerciveness properties (see [3]). Consequently, the integral problem can be discretized by unconditionally stable schemes with well-behaved stability constants even for large times [4]. The algebraic reformulation of the energetic BEM (EBEM) leads to a linear system whose matrix has a Toeplitz lower-triangular block structure, that allows the acceleration of the solution phase. As a direct consequence of the flexibility of the EBEM, a large body of literature has risen to witness its capabilities to simulate 3D acoustic (see [5]) and 2D elastodynamic (see [8, 10–12]) wave propagation in semi-infinite or infinite media. Furthermore, we recall that the energetic space–time BIEs, hence the associated potential representations, have been also used to restrict the original partial differential equation (PDE) exterior acoustic problem to a bounded region of physical interest. Indeed, this approach has allowed to construct transparent (or non-reflecting) boundary conditions on the boundary of the chosen region and to retrieve the solution of the original problem in the new exterior bounded domain by using the Finite Element Method (see [6, 7]).

In this paper, we extend the EBEM to 3D elastodynamic problems, showing the capabilities of the method of modelling a full wavefield rather than specific wave types and addressing various computational aspects of the proposed approximation method. In particular, we consider the Navier–Cauchy equation of motion, defined in bounded or unbounded domains external to 3D obstacles and endowed with a Dirichlet condition on the boundary and null initial conditions. Such problems are reformulated in terms of a space–time weakly-singular BIE of the first kind, whose energetic full space–time discretization requires double integration both in space and in time. Since a key ingredient for the success of the EBEM is the efficient and accurate evaluation of all the involved integrals, the selected formulation could be quite challenging in large scale applications. Nevertheless, if standard (constant) shape functions for time discretization are employed, the double integration in time can be performed analytically and one is left with the task of evaluating double space integrals, whose integration domains are generally delimited by the wave fronts of the primary and the secondary waves. In order to exactly detect this latter, and consequently to preserve the stability properties of the

EBEM, we choose boundary meshes made by triangular elements with straight sides and we propose an ad-hoc numerical integration scheme, tailored for the correct domain of integration. We remark that such a study has been presented in [5] in the case of 3D acoustic (scalar) wave equation but a straightforward generalization to elastic (vector) problems is not possible, due to a more involved fundamental solution and the presence of two wave fronts.

The paper is organized as follows: after presenting the model problem in the next section, we recall its energetic BIE weak formulation in Sect. 3. Then, we devote Sect. 4 to detail the energetic BEM discretization, focusing on its algebraic reformulation and on the analysis of the time-integrated kernels generating the matrix entries. In Sect. 5, we describe the numerical and analytical strategies adopted for the double space integrals at hand, with a specific attention devoted to the representation of the wave fronts of the primary and secondary waves. Numerical results validating the proposed approach are illustrated and discussed in Sect. 6. Finally, some conclusions are drawn in the last section.

## 2 Model problem

In the Euclidean space  $\mathbf{R}^3$  equipped with a fixed orthonormal Cartesian coordinates axes  $\mathbf{e}_1, \mathbf{e}_2, \mathbf{e}_3$  with origin at  $\mathbf{O} = (0, 0, 0)^\top$ , let  $\Omega_l \subset \mathbf{R}^3$  be a domain admitting a connected, smooth and orientable closed boundary surface  $\Gamma = \partial\Omega_l$ . In absence of body forces, we are interested in studying the propagation of elastic waves in a homogeneous isotropic elastic medium occupying  $\Omega_l$ . When the domain is a finite volume the problem is interior with using the notation  $l = i$ . Otherwise, it is set  $l = e$  and we study the exterior problem. Moreover, let  $\Omega = \Omega_i \cup \Omega_e = \mathbf{R}^3 \setminus \Gamma$ .

In both  $\Omega_l$ ,  $l = i, e$ , assuming small variations of the (real-valued) displacement field  $\mathbf{u}(\mathbf{x}; t) = (u_1, u_2, u_3)^\top$  at location  $\mathbf{x} = (x_1, x_2, x_3)^\top \in \Omega_l$  and time  $t \in [0, T]$ , this latter is defined by the following system:

$$\rho \ddot{\mathbf{u}}(\mathbf{x}; t) - \mu \Delta \mathbf{u}(\mathbf{x}; t) - (\lambda + \mu) \nabla \nabla \cdot \mathbf{u}(\mathbf{x}; t) = \mathbf{0} \quad (\mathbf{x}; t) \in \Omega_l \times [0, T] \quad (2.1a)$$

$$\mathbf{u}(\mathbf{x}; t) = \mathbf{g}(\mathbf{x}; t) \quad (\mathbf{x}; t) \in \Gamma \times [0, T] \quad (2.1b)$$

$$\mathbf{u}(\mathbf{x}; 0) = \mathbf{0} \quad \mathbf{x} \in \Omega_l \quad (2.1c)$$

$$\dot{\mathbf{u}}(\mathbf{x}; 0) = \mathbf{0} \quad \mathbf{x} \in \Omega_l \quad (2.1d)$$

where  $\rho$  is the mass density,  $\mu$  is the shear modulus and  $\lambda$  is the Lamé parameter. These last two quantities are related to the Poisson ratio  $\nu$  by  $\lambda := 2\mu\nu(1 - 2\nu)^{-1}$ . Furthermore, the

superposed dot indicates time differentiation, while  $\nabla$  and  $\Delta$  denote the nabla and the Laplace operators, respectively.

In the above problem, Eq. (2.1a) is known as Navier–Cauchy equation of motion, Eq. (2.1b) represents a boundary condition of Dirichlet type with datum  $\mathbf{g}(\mathbf{x}; t)$  and Eqs. (2.1c) and (2.1d) are the quiescent initial conditions, that specify the value of  $\mathbf{u}(\mathbf{x}; t)$  and  $\dot{\mathbf{u}}(\mathbf{x}; t)$  at the first time of interest  $t = 0$ .

Elastodynamics waves are characterized by primary and secondary velocities, defined by  $c_P^2 := (\lambda + 2\mu)\varrho^{-1}$ ,  $c_S^2 := \mu\varrho^{-1}$  and related, respectively, to the so-called primary or pressure waves (P-waves in short) and secondary or shear waves (S-waves in short). Since for any real materials  $-1 < \nu < 0.5$ , it's easy to verify that  $c_P > c_S$ , that is P-waves travel faster than S-waves.

In what follows, we denote by  $\sigma[\mathbf{u}](\mathbf{x}; t)$  and  $\epsilon[\mathbf{u}](\mathbf{x}; t)$  the second order stress and strain tensors, respectively. The latter is defined by the constitutive law of the linear elastic model, i.e.

$$\epsilon[\mathbf{u}](\mathbf{x}; t) = \frac{1}{2} \left[ \nabla \mathbf{u}(\mathbf{x}; t) + \nabla \mathbf{u}(\mathbf{x}; t)^\top \right] \quad (2.2)$$

and it is related to the stress tensor through the Hooke's law

$$\sigma[\mathbf{u}](\mathbf{x}; t) = \mathbf{C} : \epsilon[\mathbf{u}](\mathbf{x}; t), \quad (2.3)$$

in which the symbol “:” denotes the double tensor inner product and  $\mathbf{C}$  is the fourth order relaxation tensor, whose components are given by  $C_{ij}^{k\ell} := \lambda \delta_{ij} \delta_{k\ell} + \mu (\delta_{ik} \delta_{j\ell} + \delta_{i\ell} \delta_{jk})$  for  $i, j, k, \ell = 1, 2, 3$  ( $\delta_{ij}$  being the Kronecker symbol).

Furthermore, the traction vector  $\mathbf{p} = (p_1, p_2, p_3)^\top$  along  $\Gamma$  can be defined through the stress tensor as:

$$\mathbf{p}(\mathbf{x}; t) := \sigma[\mathbf{u}](\mathbf{x}; t) \cdot \mathbf{n}, \quad (2.4)$$

where  $\mathbf{n}$  denotes the unit normal vector to the boundary pointing outside the domain  $\Omega_l$ .

### 3 Energetic TD-BIE weak formulation

It is well known that, starting from the Somigliana identity (see [15]) written for both  $\Omega_i$  and  $\Omega_e$ , the solution of the initial boundary value problem (2.1) can be represented as single-layer potential (see [18]), i.e.

$$\mathbf{u}(\mathbf{x}; t) := \int_0^t \int_\Gamma \mathbf{G}(\mathbf{x}, \mathbf{y}; t, \tau) \mathbf{w}(\mathbf{y}; \tau) d\Gamma_y d\tau, \quad \mathbf{x} \in \Omega_l \text{ and } t \in [0, T], \quad (3.1)$$

where  $\mathbf{w} = (w_1, w_2, w_3)^\top$  is a suitable density field to be determined in the same functional space of the traction field  $\mathbf{p}$ . Furthermore, the second-order tensor  $\mathbf{G}$  satisfies the

Green's identity in relation to Navier–Cauchy operator in the left hand side of Equation (2.1a). Hence, it is the fundamental solution of the equation

$$\varrho \ddot{\mathbf{u}}(\mathbf{x}; t) - \mu \Delta \mathbf{u}(\mathbf{x}; t) - (\lambda + \mu) \nabla \nabla \cdot \mathbf{u}(\mathbf{x}; t) = \delta(\mathbf{x} - \mathbf{y}) \delta(t - \tau) \mathbf{I}, \quad (3.2)$$

where  $\mathbf{I}$  stands for the 3-by-3 identity tensor, and it represents the response at the observation point  $\mathbf{x}$  and observation time  $t$  due to a unit magnitude load, modelled by the Dirac distribution  $\delta(\cdot)$  and acting at the source point  $\mathbf{y}$  and emission time  $\tau$ . Since the coefficients in (2.1a) are independent of space and time, the components of the tensor  $\mathbf{G}$  depend on the arguments  $\mathbf{x}, \mathbf{y}, t, \tau$  only through the differences  $\mathbf{r} := \mathbf{x} - \mathbf{y}$  and  $t - \tau$ , i.e. for  $i, j = 1, 2, 3$  (see [15])

$$G_{ij}(\mathbf{x}, \mathbf{y}; t, \tau) := \frac{1}{4\pi\varrho c_P^2} \frac{r_i r_j}{r^3} \delta\left(t - \tau - \frac{r}{c_P}\right) + \frac{1}{4\pi\varrho c_S^2} \left( \frac{\delta_{ij}}{r} - \frac{r_i r_j}{r^3} \right) \delta\left(t - \tau - \frac{r}{c_S}\right) - \frac{1}{4\pi\varrho} \left( \frac{\delta_{ij}}{r^3} - \frac{r_i r_j}{r^5} \right) (t - \tau) \left[ H\left(t - \tau - \frac{r}{c_P}\right) - H\left(t - \tau - \frac{r}{c_S}\right) \right], \quad (3.3)$$

where  $r_i$  is the  $i$ -th component of  $\mathbf{r}$ , the distance  $r := |\mathbf{x} - \mathbf{y}|$  is the euclidean norm of  $\mathbf{r}$  and  $H(\cdot)$  is the Heaviside function. We remark that the expression (3.3) can be recast in the following form:

$$G_{ij}(\mathbf{x}, \mathbf{y}; t, \tau) = \frac{r_i r_j}{r^2} G_P(\mathbf{x}, \mathbf{y}; t, \tau) + \left( \delta_{ij} - \frac{r_i r_j}{r^2} \right) G_S(\mathbf{x}, \mathbf{y}; t, \tau) - \left( \delta_{ij} - 3 \frac{r_i r_j}{r^2} \right) [\tilde{G}_P(\mathbf{x}, \mathbf{y}; t, \tau) - \tilde{G}_S(\mathbf{x}, \mathbf{y}; t, \tau)], \quad (3.4)$$

in which

$$G_*(\mathbf{x}, \mathbf{y}; t, \tau) := \frac{1}{4\pi\varrho c_*^2 r} \delta\left(t - \tau - \frac{r}{c_*}\right) \text{ with } * = P, S \quad (3.5)$$

is the fundamental solution for the 3D scalar wave equation, while  $\tilde{G}_*(\mathbf{x}, \mathbf{y}; t, \tau)$  is defined by

$$\tilde{G}_*(\mathbf{x}, \mathbf{y}; t, \tau) := \frac{1}{4\pi\varrho r^3} (t - \tau) H\left(t - \tau - \frac{r}{c_*}\right) \text{ with } * = P, S. \quad (3.6)$$

216 From (3.1), with a limiting process that makes a point  $\mathbf{x} \in$   
 217  $\Omega_t$  tending to a point  $\mathbf{x} \in \Gamma$  and exploiting the Dirichlet  
 218 boundary condition, we can obtain a system of three TD-  
 219 BIEs:

$$\int_0^t \int_{\Gamma} \mathbf{G}(\mathbf{x}, \mathbf{y}; t, \tau) \mathbf{w}(\mathbf{y}; \tau) d\Gamma_{\mathbf{y}} d\tau = \mathbf{g}(\mathbf{x}; t),$$

( $\mathbf{x}; t) \in \Gamma \times [0, T]$ . (3.7)

222 For  $s \in [-1, 1]$ , let  $H^s(\Gamma)$  denote the usual fractional  
 223 order Sobolev space, with  $H^0(\Gamma) = L^2(\Gamma)$ , and  $\mathbf{H}^s(\Gamma) =$   
 224  $(H^s(\Gamma))^3$ . Referring to [10, 17, 30] for what concerns  
 225 the following functional spaces, introducing the space-  
 226 time integral operator  $\mathbf{V} : L^2([0, T]; \mathbf{H}^{-1/2}(\Gamma)) \rightarrow$   
 227  $H^1([0, T]; \mathbf{H}^{1/2}(\Gamma))$  such that:

$$\mathbf{V}[\mathbf{w}](\mathbf{x}; t) := \int_0^t \int_{\Gamma} \mathbf{G}(\mathbf{x}, \mathbf{y}; t, \tau) \mathbf{w}(\mathbf{y}; \tau) d\Gamma_{\mathbf{y}} d\tau,$$

( $\mathbf{x}; t) \in \Gamma \times [0, T]$ , (3.8)

230 the TD-BIEs (3.7) can be written with the compact notation

$$\mathbf{V}[\mathbf{w}](\mathbf{x}; t) = \mathbf{g}(\mathbf{x}; t),$$

( $\mathbf{x}; t) \in \Gamma \times [0, T]$ . (3.9)

233 The above BIE will be set in the so-called energetic weak  
 234 form. With this aim, following what has been proven in  
 235 [11] for 2D elastodynamics, which can be straightforwardly  
 236 extended to 3D space dimension, we introduce the energy  
 237 of the Navier–Cauchy equation (2.1a), which is defined as  
 238 follows:

$$\mathcal{K}(t; \mathbf{u}) := \frac{1}{2} \int_{\Omega} \varrho |\dot{\mathbf{u}}(\mathbf{x}; t)|^2 d\mathbf{x}$$

$$+ \frac{1}{2} \int_{\Omega} \boldsymbol{\sigma}[\mathbf{u}](\mathbf{x}; t) : \boldsymbol{\epsilon}[\mathbf{u}](\mathbf{x}; t) d\mathbf{x}$$

(3.10)

241 and we remark that the solution  $\mathbf{u}$  of problem (2.1) satisfies  
 242 the following energy identity

$$\mathcal{K}(T; \mathbf{u}) = \int_0^T \int_{\Gamma} \mathbf{w}^{\top}(\mathbf{x}; t) \dot{\mathbf{u}}(\mathbf{x}; t) d\Gamma_{\mathbf{x}} dt.$$

(3.11)

244 which can be obtained multiplying equation (2.1a) by  $\dot{\mathbf{u}}$  and  
 245 integrating by parts over  $\Omega \times [0, T]$ .

Having introduced the bilinear form  $\mathcal{A}_{\mathcal{K}} : L^2([0, T]; \mathbf{H}^{-1/2}(\Gamma)) \times$   
 $L^2([0, T]; \mathbf{H}^{-1/2}(\Gamma)) \rightarrow \mathbf{R}$  defined by

$$\mathcal{A}_{\mathcal{K}}(\mathbf{w}, \mathbf{v}) := \int_0^T \int_{\Gamma} \mathbf{v}^{\top}(\mathbf{x}; t) \frac{\partial}{\partial t} \mathbf{V}[\mathbf{w}](\mathbf{x}; t) d\Gamma_{\mathbf{x}} dt,$$

(3.12)

the space–time energetic weak formulation of the TD-BIEs  
 (3.9) reads as follows

find the density function  $\mathbf{w} \in L^2([0, T]; \mathbf{H}^{-1/2}(\Gamma))$  such  
 that:

$$\mathcal{A}_{\mathcal{K}}(\mathbf{w}, \mathbf{v}) = \int_0^T \int_{\Gamma} \mathbf{v}^{\top}(\mathbf{x}; t) \dot{\mathbf{g}}(\mathbf{x}; t) d\Gamma_{\mathbf{x}} dt$$

$$\forall \mathbf{v} \in L^2([0, T]; \mathbf{H}^{-1/2}(\Gamma)).$$

(3.13)

Note that  $\mathcal{A}_{\mathcal{K}}$  is defined as a quadruple integral, double in  
 space and double in time.

The above weak BIEs system is the core of the entire  
 method: its numerical resolution generates an approximation  
 of vector field  $\mathbf{w}$  that can be used in the representation formula  
 (3.1), recovering in a post-processing phase the behaviour of  
 the displacement  $\mathbf{u}$  at each point of the space domain and at  
 each time instant.

### 4 Galerkin BEM discretization

For the discretization phase, we consider a uniform decompo-  
 sition of the time interval  $[0, T]$  with time step  $\Delta_t := T/N_{\Delta_t}$ ,  
 $N_{\Delta_t}$  being a positive integer, generated by  $N_{\Delta_t} + 1$  instants:

$$t_n := n \Delta_t, \quad n = 0, \dots, N_{\Delta_t}$$

(4.1)

and we choose temporally piecewise constant shape func-  
 tions, although higher degree shape functions can be used.  
 Note that, for this particular choice, the shape functions,  
 denoted by  $\bar{v}_n(t)$ , are defined as:

$$\bar{v}_n(t) := H(t - t_n) - H(t - t_{n+1}),$$

$n = 0, \dots, N_{\Delta_t} - 1.$  (4.2)

For the space discretization, we introduce on  $\Gamma$  an admis-  
 sible triangulation  $\mathcal{T}_{\Delta_x}(\Gamma) := \{E_1, \dots, E_{M_{\Delta_x}}\}$  constituted  
 by  $M_{\Delta_x}$  flat triangular elements. The index  $\Delta_x$  denotes the  
 mesh size. We also assume that  $\cup_{i=1}^{M_{\Delta_x}} E_i$  coincides with  $\bar{\Gamma}$  if  
 the boundary is polygonal, or it is a suitable approximation  
 of  $\bar{\Gamma}$ , otherwise. The functional background compels one to  
 choose spatially shape functions whose components belong

281 to  $L^2(\Gamma)$ . Hence, we consider piecewise constant basis functions  
 282  $v_m(\mathbf{x})$ ,  $m = 1, \dots, M_{\Delta_x}$  related to  $\mathcal{T}_{\Delta_x}(\Gamma)$ . Thus, the  
 283 approximate solution of (3.13) is expressed as:

$$284 \quad \mathbf{w}(\mathbf{x}; t) \simeq \tilde{\mathbf{w}}(\mathbf{x}; t) := \sum_{n=0}^{N_{\Delta_t}-1} \tilde{v}_n(t) \sum_{m=1}^{M_{\Delta_x}} \alpha_m^{(n)} v_m(\mathbf{x})$$

$$285 \quad \text{with } \alpha_m^{(n)} := \left( \alpha_{m,1}^{(n)}, \alpha_{m,2}^{(n)}, \alpha_{m,3}^{(n)} \right)^\top \quad (4.3)$$

286 and the test functions are replaced by

$$287 \quad \mathbf{v}(\mathbf{x}; t) = v_{\tilde{m}}(\mathbf{x}) \tilde{v}_{\tilde{n}}(t) \mathbf{e}, \quad (4.4)$$

288 where  $\mathbf{e} := \mathbf{e}_1 + \mathbf{e}_2 + \mathbf{e}_3 = (1, 1, 1)^\top$ . The Galerkin BEM  
 289 discretization coming from the energetic weak formulation  
 290 (3.13) produces the linear system

$$291 \quad \mathbb{E} \boldsymbol{\alpha} = \boldsymbol{\beta}, \quad (4.5)$$

292 where the matrix  $\mathbb{E}$  has a block lower triangular Toeplitz  
 293 structure, since its elements depend on the difference  $\Delta_{\tilde{n},n} :=$   
 294  $t_{\tilde{n}} - t_n$ , and in particular they vanish if  $t_{\tilde{n}} < t_n$ . Since we deal  
 295 with 3D elastodynamic problems, if we denote by  $\mathbb{E}^{(\ell)}$  the  
 296 block obtained when  $\Delta_{\tilde{n},n} = \ell \Delta_t$ ,  $\ell = 0, \dots, N_{\Delta_t} - 1$ , we  
 297 remark that each pair of spatial indices  $\tilde{m}, m = 1, \dots, M_{\Delta_x}$   
 298 does not define a single entry of  $\mathbb{E}^{(\ell)}$  but rather a  $3 \times 3$  sub-  
 299 block  $\mathbb{E}_{\tilde{m},m}^{(\ell)}$ . Thus, each block  $\mathbb{E}^{(\ell)}$  of the matrix  $\mathbb{E}$  requires  
 300  $O((3M_{\Delta_x})^2)$  memory and computation time. Furthermore,  
 301 the evaluation of a single entry of  $\mathbb{E}_{\tilde{m},m}^{(\ell)}$  is expensive, because  
 302 we have to address the issue of computing quadruple integrals:  
 303

$$304 \quad \left( \mathbb{E}_{\tilde{m},m}^{(\ell)} \right)_{ij}$$

$$305 \quad = \int_0^T \int_{\Gamma} \frac{\partial}{\partial t} \left( \int_0^t \int_{\Gamma} G_{ij}(\mathbf{x}, \mathbf{y}; t, \tau) v_m(\mathbf{y}) \tilde{v}_n(\tau) d\Gamma_{\mathbf{y}} d\tau \right)$$

$$306 \quad v_{\tilde{m}}(\mathbf{x}) \tilde{v}_{\tilde{n}}(t) d\Gamma_{\mathbf{x}} dt$$

$$307 \quad = - \int_0^T \int_{\Gamma} \left( \int_0^t \int_{\Gamma} G_{ij}(\mathbf{x}, \mathbf{y}; t, \tau) v_m(\mathbf{y}) \dot{\tilde{v}}_n(\tau) d\Gamma_{\mathbf{y}} d\tau \right)$$

$$308 \quad v_{\tilde{m}}(\mathbf{x}) \dot{\tilde{v}}_{\tilde{n}}(t) d\Gamma_{\mathbf{x}} dt \quad (4.6)$$

309 but, after a double analytic integration in the time variables,  
 310 we obtain:

$$311 \quad \mathbb{E}_{\tilde{m},m}^{(\ell)} = -\frac{1}{4\pi\varrho} \sum_{\eta, \tilde{\eta}=0}^1 (-1)^{\eta+\tilde{\eta}} \int_{E_{\tilde{m}}} \int_{E_m} \mathbb{G}(\mathbf{x}, \mathbf{y}; \Delta_{\tilde{n}+\tilde{\eta},n+\eta})$$

$$312 \quad v_m(\mathbf{y}) v_{\tilde{m}}(\mathbf{x}) d\Gamma_{\mathbf{y}} d\Gamma_{\mathbf{x}}. \quad (4.7)$$

313 In the above relationship, the components of the time-  
 314 integrated kernel  $\mathbb{G}$  are given by

$$315 \quad \mathbb{G}_{ij}(\mathbf{x}, \mathbf{y}; \Delta_{\tilde{n},n}) = \frac{1}{c_p^2} \frac{r_i r_j}{r^3} H \left( \Delta_{\tilde{n},n} - \frac{r}{c_p} \right)$$

$$316 \quad + \frac{1}{c_s^2} \left( \frac{\delta_{ij}}{r} - \frac{r_i r_j}{r^3} \right) H \left( \Delta_{\tilde{n},n} - \frac{r}{c_s} \right) - \frac{1}{2} \left( \frac{\delta_{ij}}{r^3} - \frac{r_i r_j}{r^5} \right)$$

$$317 \quad \left[ \left( \Delta_{\tilde{n},n}^2 - \frac{r^2}{c_p^2} \right) H \left( \Delta_{\tilde{n},n} - \frac{r}{c_p} \right) \right.$$

$$318 \quad \left. - \left( \Delta_{\tilde{n},n}^2 - \frac{r^2}{c_s^2} \right) H \left( \Delta_{\tilde{n},n} - \frac{r}{c_s} \right) \right] \quad (4.8)$$

316 where the Heaviside functions represent the wave front prop-  
 317 agation and their contribution is 0 or 1. If  $r < c_s \Delta_{\tilde{n},n} <$   
 318  $c_p \Delta_{\tilde{n},n}$ , then (4.8) reduces to

$$319 \quad \mathbb{G}_{ij}(\mathbf{x}, \mathbf{y}; \Delta_{\tilde{n},n})$$

$$320 \quad = \frac{1}{2} \left( \frac{r_i r_j c_p^2 - c_s^2}{r^3 c_p^2 c_s^2} + \frac{\delta_{ij} c_p^2 + c_s^2}{r c_p^2 c_s^2} \right) \quad (4.9)$$

321 and we observe a space singularity of type  $\mathcal{O}(1/r)$  as  $r \rightarrow 0$ ,  
 322 which is typical of weakly singular kernels related to 3D elliptic  
 323 problems. Moreover, when  $0 < c_s \Delta_{\tilde{n},n} < r < c_p \Delta_{\tilde{n},n}$ ,  
 324 (4.8) is no longer singular and becomes

$$325 \quad \mathbb{G}_{ij}(\mathbf{x}, \mathbf{y}; \Delta_{\tilde{n},n})$$

$$326 \quad = \frac{1}{2} \left( \frac{1}{c_p^2} \frac{\delta_{ij}}{r} - \frac{1}{c_p^2} \frac{r_i r_j}{r^3} - \frac{\delta_{ij}}{r^3} \Delta_{\tilde{n},n}^2 + 3 \frac{r_i r_j}{r^5} \Delta_{\tilde{n},n}^2 \right). \quad (4.10)$$

328 Combining (4.7) and (4.9), it easy to show that, if  $N^*$  denotes  
 329 the first time index such that  $c_p t_{N^*-1} > c_s t_{N^*-1} > \text{diam}(\Gamma)$ ,  
 330 we have  $\mathbb{E}_{\tilde{m},m}^{(\ell)} = 0$  for all  $\ell = N^*, \dots, N_{\Delta_t}-1$ . Due to this  
 331 cut-off property, the matrix of the final linear system (4.5)  
 332 has the well known band structure of standard collocation  
 333 approaches [28], i.e.

$$\begin{pmatrix}
 \mathbf{E}^{(0)} & 0 & 0 & 0 & 0 & 0 & 0 & \dots & 0 \\
 \mathbf{E}^{(1)} & \mathbf{E}^{(0)} & 0 & 0 & 0 & 0 & 0 & \dots & 0 \\
 \mathbf{E}^{(2)} & \mathbf{E}^{(1)} & \mathbf{E}^{(0)} & 0 & 0 & 0 & 0 & \dots & 0 \\
 \vdots & \vdots & \vdots & \ddots & \ddots & \vdots & \vdots & \vdots & \vdots \\
 \mathbf{E}^{(N^*-1)} & \mathbf{E}^{(N^*-2)} & \mathbf{E}^{(N^*-3)} & \dots & \mathbf{E}^{(0)} & 0 & 0 & \dots & 0 \\
 0 & \mathbf{E}^{(N^*-1)} & \mathbf{E}^{(N^*-2)} & \mathbf{E}^{(N^*-3)} & \dots & \mathbf{E}^{(0)} & 0 & \dots & 0 \\
 0 & 0 & \mathbf{E}^{(N^*-1)} & \mathbf{E}^{(N^*-2)} & \mathbf{E}^{(N^*-3)} & \dots & \mathbf{E}^{(0)} & \dots & 0 \\
 \vdots & \vdots & \ddots & \ddots & \ddots & \ddots & \ddots & \ddots & \vdots \\
 0 & 0 & \dots & 0 & \mathbf{E}^{(N^*-1)} & \mathbf{E}^{(N^*-2)} & \mathbf{E}^{(N^*-3)} & \dots & \mathbf{E}^{(0)}
 \end{pmatrix} \quad (4.11)$$

while the unknowns and right hand side entries are organized as follows

$$\begin{aligned}
 \boldsymbol{\alpha} &= (\boldsymbol{\alpha}^{(0)}, \boldsymbol{\alpha}^{(1)}, \dots, \boldsymbol{\alpha}^{(N^*)}, \dots, \boldsymbol{\alpha}^{(N_{\Delta t}-1)})^\top \\
 &\text{with } \boldsymbol{\alpha}^{(\ell)} = (\alpha_1^{(\ell)}, \alpha_2^{(\ell)}, \dots, \alpha_{M_{\Delta x}}^{(\ell)})^\top \\
 \boldsymbol{\beta} &= (\boldsymbol{\beta}^{(0)}, \boldsymbol{\beta}^{(1)}, \dots, \boldsymbol{\beta}^{(N^*)}, \dots, \boldsymbol{\beta}^{(N_{\Delta t}-1)})^\top \\
 &\text{with } \boldsymbol{\beta}^{(\ell)} = (\beta_1^{(\ell)}, \beta_2^{(\ell)}, \dots, \beta_{M_{\Delta x}}^{(\ell)})^\top.
 \end{aligned} \quad (4.12)$$

The solution of (4.11) is obtained by a block forward substitution, i.e. at every time instant  $t_\ell$ , with  $\ell = 0, \dots, N_{\Delta t} - 1$ , one computes

$$\begin{aligned}
 \mathbf{z}^{(\ell)} &= \boldsymbol{\beta}^{(\ell)} - \sum_{j=1}^{\ell^*} \mathbf{E}^{(j)} \boldsymbol{\alpha}^{(\ell-j)} \\
 &\text{with } \ell^* := \min \{ \ell, N^* - 1 \},
 \end{aligned} \quad (4.13)$$

and then solves the reduced linear system

$$\mathbf{E}^{(0)} \boldsymbol{\alpha}^{(\ell)} = \mathbf{z}^{(\ell)}. \quad (4.14)$$

Procedure (4.13) and (4.14) is a time-marching technique, where the only matrix to be inverted is the non-singular block  $\mathbf{E}^{(0)}$ ; therefore the LU factorization needs to be performed only once and stored. Then, at each time step, the solution of (4.14) requires only a forward and a backward substitution phases. All the other blocks  $\mathbf{E}^{(\ell)}$ , with  $\ell = 1, \dots, N^* - 1$ , are used to update at every time step the right-hand side. Of course, due to the whole matrix  $\mathbf{E}$  structure, one can construct and store only blocks  $\mathbf{E}^{(0)}, \dots, \mathbf{E}^{(N^*-1)}$  with a considerable reduction in the computational cost and the memory requirement.

**Remark** We stress that the crucial point for the success of the energetic BEM is the careful numerical evaluation of the entries of the block  $\mathbf{E}^{(0)}$  that must take place under the assumption that all the involved integrals are computed with a sufficiently high accuracy.

**Remark** The proposed energetic weak formulation, after time integration, can be regarded as a Newmark scheme with parameters  $\zeta = 1/2$  and  $\theta = 1$  in the notation of [33], as proved for scalar problems in [6, 7] in the more general framework of Energetic BEM-FEM coupling. This particular Newmark scheme is implicit, unconditionally stable and first-order accurate in  $\Delta t$ . Furthermore, the theoretical analysis about convergence and space-time accuracy in the context of 3D elastodynamic problems has been performed in [10].

### 5 Quadrature of double integrals in space variables

In this section we focus on the efficient computation of the space integrals appearing in (4.7), which is essential for the numerical stability of the EBEM. Since we use piecewise constant basis and test functions, we can reduce the integrals over  $\Gamma$  to double integrals over the source and the field triangles  $E_{\bar{m}}$  and  $E_m$  respectively:

$$\mathbb{E}_{\bar{m},m}^{(\ell)} = -\frac{1}{4\pi Q} \sum_{\eta, \bar{\eta}=0}^1 (-1)^{\eta+\bar{\eta}} \int_{E_{\bar{m}}} \int_{E_m} \mathbb{G}(\mathbf{x}, \mathbf{y}; \Delta_{\bar{n}+\bar{\eta}, n+\eta}) d\Gamma_{\mathbf{y}} d\Gamma_{\mathbf{x}}. \quad (5.1)$$

The outer integration on the source triangle is carried out by applying a  $M_g$ -point suitable quadrature rule, so that

$$\mathbb{E}_{\bar{m},m}^{(\ell)} \simeq -\frac{1}{4\pi Q} \sum_{\eta, \bar{\eta}=0}^1 (-1)^{\eta+\bar{\eta}} \sum_{q=1}^{M_g} \omega_q \int_{E_m} \mathbb{G}(\mathbf{x}_q, \mathbf{y}; \Delta_{\bar{n}+\bar{\eta}, n+\eta}) d\Gamma_{\mathbf{y}}, \quad (5.2)$$

where  $\mathbf{x}_q$  and  $\omega_q$  are the quadrature nodes and weights, respectively. The same strategy can in principle be used for

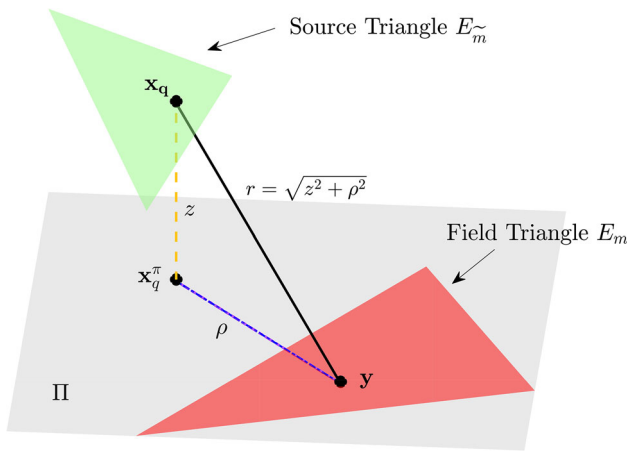


Fig. 1 Projection of the source point  $\mathbf{x}_q$  onto the plane of the inner (field) triangle of integration

nates system and the corresponding kernel  $\hat{\mathbb{G}}$  with respect to the new coordinates system, i.e.  $\mathbb{G} = \mathbb{S}^{-1}\hat{\mathbb{G}}\mathbb{S}$ . As the consequence, we obtain:

$$\mathbb{E}_{\tilde{m},m}^{(\ell)} \simeq -\frac{1}{4\pi\varrho} \sum_{\eta,\tilde{\eta}=0}^1 (-1)^{\eta+\tilde{\eta}} \sum_{q=1}^v \omega_q \int_{\hat{E}_m} \mathbb{S}^{-1}\hat{\mathbb{G}}(\hat{\mathbf{x}}_q, \hat{\mathbf{y}}; \Delta_{\tilde{n}+\tilde{\eta},n+\eta}) \mathbb{S}d\Gamma\hat{\mathbf{y}}. \tag{5.4}$$

At this stage, we express the inner integration over the field triangle  $\hat{E}_m$  (father) as an algebraic sum of integrals over three triangles  $\hat{E}_m^{(k)}$  (children),  $k = 1, 2, 3$ , having  $\hat{\mathbf{O}}, \hat{\mathbf{y}}_1^{(k)}$  and  $\hat{\mathbf{y}}_2^{(k)}$  as vertices (see Fig. 2). Consequently, we have:

$$\mathbb{E}_{\tilde{m},m}^{(\ell)} \simeq -\frac{1}{4\pi\varrho} \sum_{\eta,\tilde{\eta}=0}^1 (-1)^{\eta+\tilde{\eta}} \sum_{q=1}^v \omega_q \sum_{k=1}^3 \varsigma_k \int_{\hat{E}_m^{(k)}} \mathbb{S}^{-1}\hat{\mathbb{G}}(\hat{\mathbf{x}}_q, \hat{\mathbf{y}}; \Delta_{\tilde{n}+\tilde{\eta},n+\eta}) \mathbb{S}d\Gamma\hat{\mathbf{y}}, \tag{5.5}$$

where the coefficients  $\varsigma_k$  are given by

$$\varsigma_k := \text{sign} \left( \begin{vmatrix} 1 & 0 & 0 \\ 1 & \hat{y}_{1,1}^{(k)} & \hat{y}_{1,2}^{(k)} \\ 1 & \hat{y}_{2,1}^{(k)} & \hat{y}_{2,2}^{(k)} \end{vmatrix} \right) = \begin{cases} -1, & \text{if } \hat{y}_{1,1}^{(k)}\hat{y}_{2,2}^{(k)} - \hat{y}_{1,2}^{(k)}\hat{y}_{2,1}^{(k)} < 0 \\ 0, & \text{if } \hat{y}_{1,1}^{(k)}\hat{y}_{2,2}^{(k)} - \hat{y}_{1,2}^{(k)}\hat{y}_{2,1}^{(k)} = 0 \\ 1, & \text{if } \hat{y}_{1,1}^{(k)}\hat{y}_{2,2}^{(k)} - \hat{y}_{1,2}^{(k)}\hat{y}_{2,1}^{(k)} > 0. \end{cases}$$

Each of the children triangles is now addressed separately. For a given  $\hat{E}_m^{(k)}$ , the lengths of its sides are defined to be:

$$a := |\hat{\mathbf{y}}_1^{(k)} - \hat{\mathbf{O}}|, \quad b := |\hat{\mathbf{y}}_2^{(k)} - \hat{\mathbf{O}}| \text{ and } c := |\hat{\mathbf{y}}_2^{(k)} - \hat{\mathbf{y}}_1^{(k)}|,$$

while its angles are defined via Carnot's theorem as

$$\alpha = \text{acos}\left(\frac{b^2 + c^2 - a^2}{2bc}\right), \quad \beta = \text{acos}\left(\frac{a^2 + c^2 - b^2}{2ac}\right) \text{ and } \gamma = \text{acos}\left(\frac{a^2 + b^2 - c^2}{2ab}\right)$$

with  $0 \leq \alpha, \beta, \gamma \leq \pi$  and  $\alpha + \beta + \gamma = \pi$ .

We make a counterclockwise rotation in the plane  $\Pi$  by an angle  $\delta$  about the  $\hat{\mathbf{e}}_3$ -axis, so that we introduce a new coordinate frame consisting of the origin  $\check{\mathbf{O}} = \hat{\mathbf{O}}$  and mutually orthogonal axes in the directions of the unit vectors  $\check{\mathbf{e}}_1, \check{\mathbf{e}}_2$  and  $\check{\mathbf{e}}_3 = \hat{\mathbf{e}}_3$ . This change of variable, which maps the point  $\hat{\mathbf{y}}_1^{(k)}$

the numerical computation of the integral over the field triangle but standard quadrature formulas would require a very large number of quadrature nodes, due to the low regularity of the time integrated kernel. Furthermore, it is worth noting that, in this case, the implementation is complicated since the integration domain is defined by the intersection of the field triangle and the wavefronts of the P- and S-waves. In particular, the presence of the Heaviside functions in (4.8) implies that the integration over  $E_m$  has to be in general limited to the portion enclosed between two spherical surfaces of radii  $r_P = c_P\Delta_{\tilde{n},n}$  and  $r_S = c_S\Delta_{\tilde{n},n}$  respectively, both centered at  $\mathbf{x}_q$ . In order to avoid excessive simplifications in dealing with such integration domains, that may strongly affect the stability properties of the EBEM, we follow the strategy suggested in [29] for the scalar wave equation. First of all, we project the source point  $\mathbf{x}_q$  into the plane  $\Pi$  containing the triangle  $E_m$  and we call  $\mathbf{x}_q^\pi$  the projection point, as depicted in Fig. 1.

Then, we apply a coordinate transformation maintaining the distances and mapping the point  $\mathbf{x}_q^\pi$  into the origin  $\hat{\mathbf{O}} = (0, 0, 0)$  and the canonical system  $\mathbf{e}_1, \mathbf{e}_2, \mathbf{e}_3$  of the Euclidean space  $\mathbf{R}^3$  into the triplet  $\hat{\mathbf{e}}_1, \hat{\mathbf{e}}_2, \hat{\mathbf{e}}_3$  where  $\hat{\mathbf{e}}_3$  is the direction perpendicular to the plane  $\Pi$  while  $\hat{\mathbf{e}}_1$  is parallel to a chosen side of the field triangle  $E_m$ . As a consequence, we have that the new coordinates of  $\mathbf{x}_q$  are  $\hat{\mathbf{x}}_q = (0, 0, z)$ , where  $z := |\mathbf{x}_q - \mathbf{x}_q^\pi|$ . This transformation is a translation and a rotation, so that the arbitrary point  $\mathbf{y} = (y_1, y_2, y_3)$  is mapped into the point  $\hat{\mathbf{y}} = (\hat{y}_1, \hat{y}_2, \hat{y}_3)$  related to it through the relations:

$$\mathbf{y} = \mathbf{x}_q^\pi + \mathbb{S}\hat{\mathbf{y}} \text{ and } \hat{\mathbf{y}} = \mathbb{S}^{-1}(\mathbf{y} - \mathbf{x}_q^\pi), \tag{5.3}$$

where  $\mathbb{S}$  is the orthogonal rotation matrix with  $|\det(\mathbb{S})| = 1$ . Considering the change of variable in (5.3), we derive the relation between the kernel  $\mathbb{G}$  with respect to the old coordi-

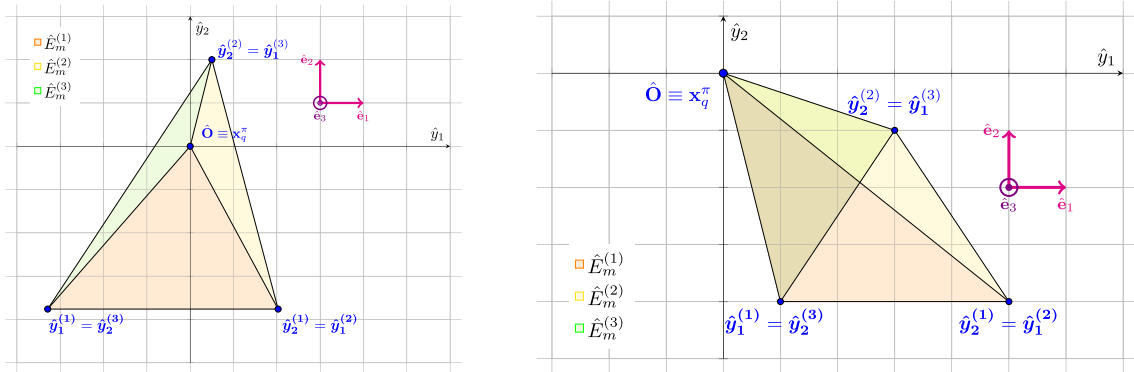


**Fig. 2** Decomposition of the field triangle  $\hat{E}_m$  (father) into three triangles  $\hat{E}_m^{(k)}$  (children),  $k = 1, 2, 3$ , having  $\hat{\mathbf{O}}, \hat{\mathbf{y}}_1^{(k)}$  and  $\hat{\mathbf{y}}_2^{(k)}$  as vertices. On the left plot, the point  $\hat{\mathbf{O}} \equiv \hat{\mathbf{x}}_q$  is inside the triangle  $\hat{E}_m$ . On the right plot, the point  $\hat{\mathbf{O}} \equiv \hat{\mathbf{x}}_q$  is outside the triangle  $\hat{E}_m$

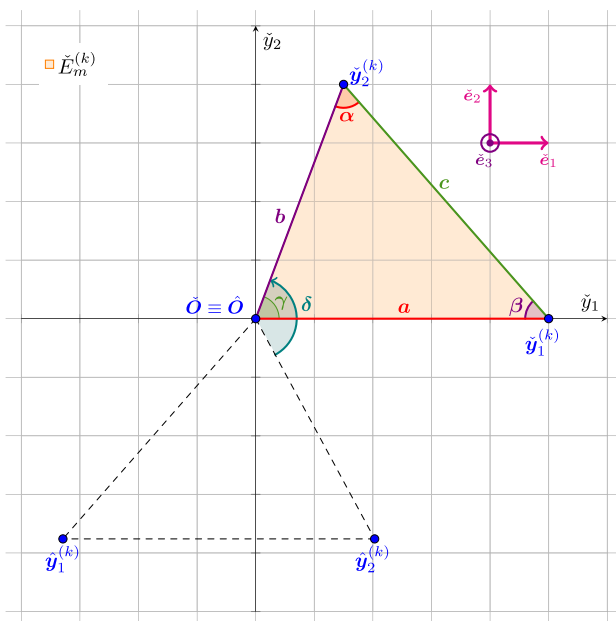


**Fig. 3** Counterclockwise rotation in the plane  $\Pi$  by an angle  $\delta$  about the  $\hat{\mathbf{e}}_3$ -axis. The new coordinate frame has the origin at  $\hat{\mathbf{O}} \equiv \hat{\mathbf{O}}$  and mutually orthogonal axes in the directions of the unit vectors  $\hat{\mathbf{e}}_1, \hat{\mathbf{e}}_2$  and  $\hat{\mathbf{e}}_3 = \hat{\mathbf{e}}_3$

$$\int_{\hat{E}_m^{(k)}} \mathbb{S}^{-1} \mathbb{T}^{-1} \check{\mathbb{G}}(\check{\mathbf{x}}_q, \check{\mathbf{y}}; \Delta_{\check{n}+\check{\eta}, n+\eta}) \mathbb{T} \mathbb{S} d\Gamma \check{\mathbf{y}}. \quad (5.7)$$

We point out that the benefits of the above described apparently cumbersome procedure are extremely significant. In fact, it is worth noting that it allows for the exact detection of the integration domain and, consequently, for the analytical computation of the integrals in (5.7), as we will explain in the following subsections.

### 5.1 Exact representation of the wave fronts

As  $z$  is constant for the integral over  $\hat{E}_m^{(k)}$ , we fix the plane  $\hat{\mathbf{e}}_1$ - $\hat{\mathbf{e}}_2$  as a working plane and we select an intrinsic 2D polar coordinate system  $(\rho, \theta)$  with origin at  $\check{\mathbf{O}} := (0, 0)$ , so that the distance  $\check{r} = |\check{\mathbf{x}}_q - \check{\mathbf{y}}|$  becomes  $\check{r} = \sqrt{z^2 + \rho^2}$ , while the components of the distance vector  $\check{\mathbf{r}} = \check{\mathbf{x}}_q - \check{\mathbf{y}}$  are given by:

$$\check{r}_i = \frac{\rho}{\sin \gamma} [A_{1i} \sin(\gamma - \theta) + A_{2i} \sin(\theta)] + A_{3i} z, \quad i = 1, 2, 3, \quad (5.8)$$

where the coefficients  $A_{1i}, A_{2i}$  and  $A_{3i}$  are defined as follows:

$$A_{1i} := \frac{1}{a} \check{\mathbf{y}}_1^{(k)} \cdot \check{\mathbf{e}}_i, \quad A_{2i} := \frac{1}{b} \check{\mathbf{y}}_2^{(k)} \cdot \check{\mathbf{e}}_i$$

and  $A_{3i} := \frac{1}{z} (\check{\mathbf{x}}_q - \check{\mathbf{O}}) \cdot \check{\mathbf{e}}_i.$

into the point  $\check{\mathbf{y}}_1^{(k)} = (a, 0, 0)$ , is represented by the matrix equations:

$$\hat{\mathbf{y}} = \mathbb{T} \check{\mathbf{y}} \quad \text{and} \quad \check{\mathbf{y}} = \mathbb{T}^{-1} \hat{\mathbf{y}}, \quad \text{with} \quad |\det(\mathbb{T})| = 1 \quad (5.6)$$

as depicted in Fig. 3. Therefore, Eq. (5.5) is recast in the following form

$$\mathbb{E}_{\check{m}, m}^{(\ell)} \simeq -\frac{1}{4\pi Q} \sum_{\eta, \check{\eta}=0}^1 (-1)^{\eta+\check{\eta}} \sum_{q=1}^v \omega_q \sum_{k=1}^3 \varsigma_k$$

471 As a consequence of relation (5.8), for each  $i, j = 1, 2, 3$  we  
 472 have

$$\begin{aligned} \check{r}_i \check{r}_j &= \frac{\rho^2}{\sin^2 \gamma} \left[ A_{1i} A_{1j} \sin^2 (\gamma - \theta) + (A_{1i} A_{2j} + A_{2i} A_{1j}) \right. \\ &\quad \left. \sin (\gamma - \theta) \sin (\theta) + A_{2i} A_{2j} \sin^2 \theta \right] \\ &+ z \frac{\rho}{\sin \gamma} \left[ (A_{1i} A_{3j} + A_{3i} A_{1j}) \sin (\gamma - \theta) \right. \\ &\quad \left. + (A_{2i} A_{3j} + A_{3i} A_{2j}) \sin \theta \right] + z^2 A_{3i} A_{3j}. \end{aligned} \tag{5.9}$$

474 Furthermore, the distance  $R(\theta)$  between a point  $\check{y}$  on the side  
 475  $\check{y}_2^{(k)} - \check{y}_1^{(k)}$  and the origin  $\check{O}$  is of particular importance for  
 476 integration purposes and it is given by

$$\begin{aligned} R(\theta) &:= \frac{F}{\sin (\theta + \beta)} \\ &\text{with } F = a \sin \beta \text{ and } \theta \in (-\beta, \pi - \beta). \end{aligned}$$

479 In order to establish a simple and general procedure to  
 480 account for the presence of the wavefronts in an exact way,  
 481 we remark that in the working plane they are represented by  
 482 two circles of radii  $\rho_P = \sqrt{r_P^2 - z^2}$  and  $\rho_S = \sqrt{r_S^2 - z^2}$ , both  
 483 centred at  $\check{O}$ . Moreover, when  $r_S < z < r_P$ , only the P-wave  
 484 front intersects the plane  $\Pi$ , inducing the partition of  $\check{E}_m^{(k)}$   
 485 depicted in the left plot of Fig. 4 and represented by (the sum of)  
 486 the three possible sub-regions:

$$\begin{aligned} \mathcal{R}_1 &:= \{(\rho, \theta) \mid \theta \in [0, \min\{\max\{0, \theta_1\}, \gamma\}], \rho \in [0, \rho_P]\} \\ \mathcal{R}_2 &:= \{(\rho, \theta) \mid \theta \in [\min\{\max\{0, \theta_1\}, \gamma\}, \max\{0, \min\{\theta_2, \gamma\}\}], \\ &\quad \rho \in [0, R(\theta)]\} \\ \mathcal{R}_3 &:= \{(\rho, \theta) \mid \theta \in [\max\{0, \min\{\theta_2, \gamma\}\}, \gamma], \rho \in [0, \rho_P]\} \end{aligned}$$

491 where the angles  $\theta_1$  and  $\theta_2$  are the slopes of the rays joining  
 492 the origin  $\check{O}$  with all the intersections between the P-wave  
 493 front and the whole extension line of the side  $\check{y}_2^{(k)} - \check{y}_1^{(k)}$   
 494 of the triangle  $\check{E}_m^{(k)}$ . Note that these intersections may lie outside  
 495 the triangle.

496 Otherwise, i.e. when  $z < r_S < r_P$ , both the P- and the S-wave  
 497 fronts are active. As a consequence, this scenario is more  
 498 complicated than the previous one, because the integration  
 499 domain (as illustrated in the right plot of Fig. 4) is made by  
 500 the seven possible sub-regions

$$\begin{aligned} \mathcal{Q}_1 &:= \{(\rho, \theta) \mid \theta \in [0, \min\{\max\{0, \theta_1\}, \gamma\}], \rho \in [0, \rho_S]\} \\ \mathcal{Q}_2 &:= \{(\rho, \theta) \mid \theta \in [\min\{\max\{0, \theta_1\}, \gamma\}, \max\{0, \min\{\theta_2, \gamma\}\}], \\ &\quad \rho \in [0, R(\theta)]\} \\ \mathcal{Q}_3 &:= \{(\rho, \theta) \mid \theta \in [\max\{0, \min\{\theta_2, \gamma\}\}, \gamma], \\ &\quad \rho \in [0, \rho_S]\} \\ \mathcal{Q}_4 &:= \{(\rho, \theta) \mid \theta \in [0, \min\{\max\{0, \theta_3\}, \gamma\}], \\ &\quad \rho \in [\rho_S, \rho_P]\} \end{aligned}$$

$$\mathcal{Q}_5 := \{(\rho, \theta) \mid \theta \in [\min\{\max\{0, \theta_3\}, \gamma\}, \min\{\max\{0, \theta_1\}, \gamma\}], \rho \in [\rho_S, R(\theta)]\}$$

$$\mathcal{Q}_6 := \{(\rho, \theta) \mid \theta \in [\max\{0, \min\{\theta_2, \gamma\}\}, \max\{0, \min\{\theta_4, \gamma\}\}], \rho \in [\rho_S, R(\theta)]\}$$

$$\mathcal{Q}_7 := \{(\rho, \theta) \mid \theta \in [\max\{0, \min\{\theta_4, \gamma\}\}, \gamma], \rho \in [\rho_S, \rho_P]\}$$

513 where the angles  $\theta_1, \theta_2, \theta_3$  and  $\theta_4$  are the slopes of the rays  
 514 joining the origin  $\check{O}$  with all the intersections between the P-  
 515 and S-wave fronts and the whole extension line of the side  
 516  $\check{y}_2^{(k)} - \check{y}_1^{(k)}$  of the triangle  $\check{E}_m^{(k)}$ .

517 Looking at Fig. 4, we remark that the sub-regions may be  
 518 traced back to four different shapes. For this reason, in order  
 519 to describe the analytical procedure to compute the integrals  
 520 in (5.7), we refer to the four reference integration domains  
 521 illustrated in Fig. 5, i.e.

$$\begin{aligned} \mathcal{E} &:= \{(\rho, \theta) \mid \theta_\spadesuit \leq \theta \leq \theta_\heartsuit \text{ and } 0 \leq \rho \leq \rho_\clubsuit\} \\ \mathcal{F} &:= \{(\rho, \theta) \mid \theta_\spadesuit \leq \theta \leq \theta_\heartsuit \text{ and } \rho_\clubsuit \leq \rho \leq \rho_\spadesuit\} \\ \mathcal{G} &:= \{(\rho, \theta) \mid \theta_\spadesuit \leq \theta \leq \theta_\heartsuit \text{ and } 0 \leq \rho \leq R(\theta)\} \\ \mathcal{H} &:= \{(\rho, \theta) \mid \theta_\spadesuit \leq \theta \leq \theta_\heartsuit \text{ and } \rho_\clubsuit \leq \rho \leq R(\theta)\}. \end{aligned}$$

526 We point out that, when  $\rho_\clubsuit = 0$ , the regions  $\mathcal{F}$  and  $\mathcal{H}$   
 527 collapse into  $\mathcal{E}$  and  $\mathcal{G}$ , respectively. For this reason, we are  
 528 going to detail the analytical integration only over the former  
 529 domains, i.e. we are going to consider

$$\begin{aligned} I_1^{\mathcal{D}} &:= \int_{\mathcal{D}} \frac{1}{\check{r}} d\Gamma_{\check{y}}, \quad I_2^{\mathcal{D}} := \int_{\mathcal{D}} \frac{\check{r}_i \check{r}_j}{\check{r}^3} d\Gamma_{\check{y}}, \\ I_3^{\mathcal{D}} &:= \int_{\mathcal{D}} \frac{\check{r}_i \check{r}_j}{\check{r}^5} d\Gamma_{\check{y}} \quad \text{and} \quad I_4^{\mathcal{D}} := \int_{\mathcal{D}} \frac{1}{\check{r}^3} d\Gamma_{\check{y}}, \end{aligned} \tag{5.10}$$

532 with  $\mathcal{D} = \mathcal{F}, \mathcal{H}$ . Since both the integration domains are  
 533 described in terms of polar coordinates, we convert the above  
 534 integrals, taking into account (5.9) and remembering that  
 535 the elemental area  $d\Gamma_{\check{y}}$  changes according to the formula  
 536  $d\Gamma_{\check{y}} = \rho d\rho d\theta$ . We point out that the results presented in the  
 537 following two sub-sections extend those in [31].

### 5.2 Integrals over the region $\mathcal{F}$

539 When  $\mathcal{D} = \mathcal{F}$ , plugging the polar coordinates into the double  
 540 integrals in (5.10) gives rise to separable integrals of the type:

$$\begin{aligned} &\int_{\theta_\spadesuit}^{\theta_\heartsuit} (\sin \theta)^{k-1} (\sin (\gamma - \theta))^{h-1} d\vartheta \int_{\rho_\clubsuit}^{\rho_\spadesuit} \frac{\rho^i}{(\rho^2 + z^2)^{j/2}} d\rho \\ &:= \Theta_{k,h}(\theta_\spadesuit, \theta_\heartsuit) K_{i,j}(\rho_\clubsuit, \rho_\spadesuit), \end{aligned}$$

543 where the indices  $h, k = 1, 2, 3$  are such that  $2 \leq h + k < 5$ ,  
 544 while the indices  $i$  and  $j$  are such that  $i = j = 1$  or  $i = 1, 2, 3$

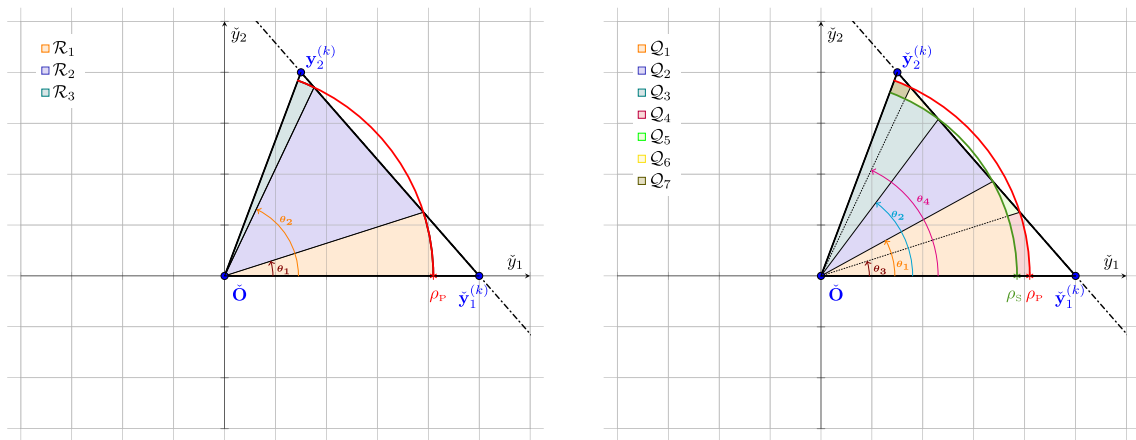
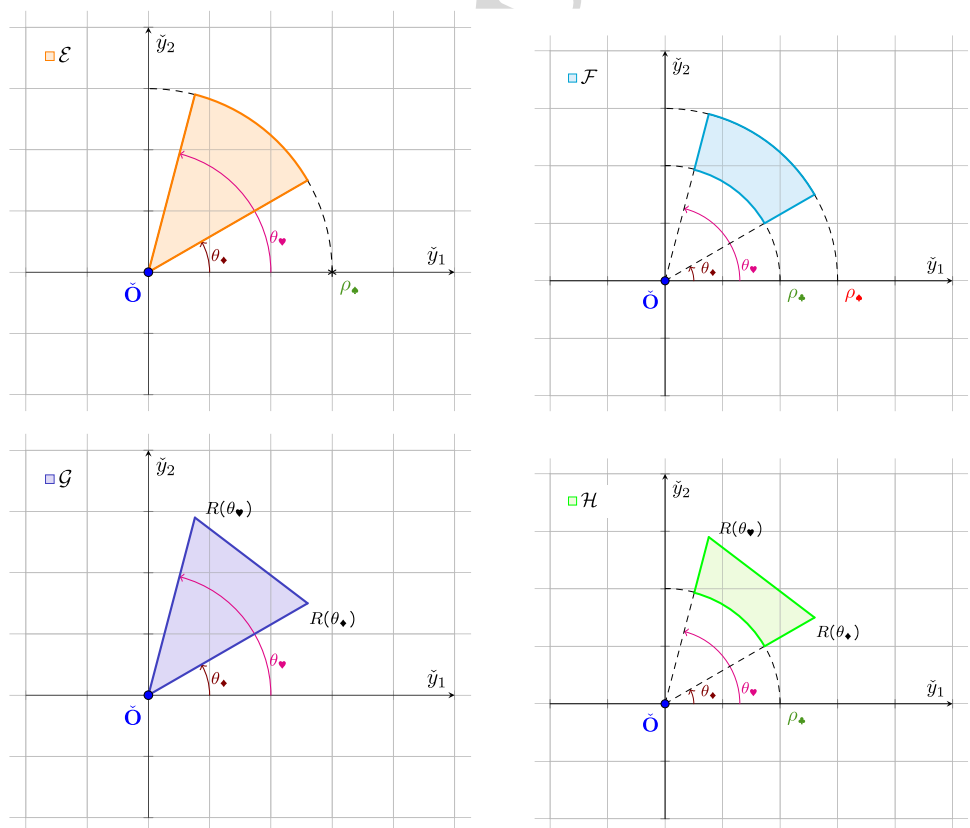


Fig. 4 General partition of one triangle  $\check{E}_m^{(k)}$  due to the wave fronts. On the left plot, only the P-wave front is active. On the right plot, both the P-wave and S-wave fronts are active

Fig. 5 The four reference integration domains



545 and  $j = 3, 5$ . It easy to check that the integration in variable  
 546  $\varrho$  produces the functions:

547 
$$K_{1,1}(\rho_{\clubsuit}, \rho_{\spadesuit}) := \sqrt{\rho_{\clubsuit}^2 + z^2} - \sqrt{\rho_{\spadesuit}^2 + z^2}$$

548 
$$K_{1,3}(\rho_{\clubsuit}, \rho_{\spadesuit}) := -\frac{1}{\sqrt{\rho_{\clubsuit}^2 + z^2}} + \frac{1}{\sqrt{\rho_{\spadesuit}^2 + z^2}}$$

549 
$$K_{1,5}(\rho_{\clubsuit}, \rho_{\spadesuit}) := \frac{1}{3} \left[ \left( \frac{1}{\sqrt{\rho_{\clubsuit}^2 + z^2}} \right)^3 - \left( \frac{1}{\sqrt{\rho_{\spadesuit}^2 + z^2}} \right)^3 \right]$$

550 
$$K_{2,3}(\rho_{\clubsuit}, \rho_{\spadesuit}) := \log \left( \frac{\rho_{\spadesuit} + \sqrt{\rho_{\spadesuit}^2 + z^2}}{\rho_{\clubsuit} + \sqrt{\rho_{\clubsuit}^2 + z^2}} \right) - \frac{\rho_{\clubsuit}}{\sqrt{\rho_{\clubsuit}^2 + z^2}} + \frac{\rho_{\spadesuit}}{\sqrt{\rho_{\spadesuit}^2 + z^2}}$$

551

552 
$$K_{2,5}(\rho_{\clubsuit}, \rho_{\spadesuit}) := \frac{1}{3z^2}$$

$$\begin{aligned}
 & \left[ \left( \frac{\rho_{\clubsuit}}{\sqrt{\rho_{\clubsuit}^2 + z^2}} \right)^3 - \left( \frac{\rho_{\spadesuit}}{\sqrt{\rho_{\spadesuit}^2 + z^2}} \right)^3 \right] \\
 K_{3,3}(\rho_{\clubsuit}, \rho_{\spadesuit}) & := \sqrt{\rho_{\clubsuit}^2 + z^2} - \sqrt{\rho_{\spadesuit}^2 + z^2} + z^2 \\
 & \left( \frac{1}{\sqrt{\rho_{\clubsuit}^2 + z^2}} - \frac{1}{\sqrt{\rho_{\spadesuit}^2 + z^2}} \right) \\
 K_{3,5}(\rho_{\clubsuit}, \rho_{\spadesuit}) & := \frac{1}{\sqrt{\rho_{\clubsuit}^2 + z^2}} - \frac{1}{\sqrt{\rho_{\spadesuit}^2 + z^2}} + \frac{z^2}{3} \\
 & \left[ \left( \frac{1}{\sqrt{\rho_{\clubsuit}^2 + z^2}} \right)^3 - \left( \frac{1}{\sqrt{\rho_{\spadesuit}^2 + z^2}} \right)^3 \right]
 \end{aligned}$$

while the results of the integration in variable  $\theta$  are:

$$\begin{aligned}
 \Theta_{1,1}(\theta_{\spadesuit}, \theta_{\heartsuit}) & := \theta_{\heartsuit} - \theta_{\spadesuit} \\
 \Theta_{1,2}(\theta_{\spadesuit}, \theta_{\heartsuit}) & := 2 \sin\left(\frac{\theta_{\heartsuit} - \theta_{\spadesuit}}{2}\right) \sin\left(\gamma - \frac{\theta_{\heartsuit} + \theta_{\spadesuit}}{2}\right) \\
 \Theta_{1,3}(\theta_{\spadesuit}, \theta_{\heartsuit}) & := \frac{1}{2} [\theta_{\heartsuit} - \theta_{\spadesuit} - \sin(\theta_{\heartsuit} - \theta_{\spadesuit}) \cos(2\gamma - \theta_{\heartsuit} - \theta_{\spadesuit})] \\
 \Theta_{2,1}(\theta_{\spadesuit}, \theta_{\heartsuit}) & := 2 \sin\left(\frac{\theta_{\heartsuit} - \theta_{\spadesuit}}{2}\right) \sin\left(\frac{\theta_{\heartsuit} + \theta_{\spadesuit}}{2}\right) \\
 \Theta_{2,2}(\theta_{\spadesuit}, \theta_{\heartsuit}) & := \frac{1}{2} [\sin(\theta_{\heartsuit} - \theta_{\spadesuit}) \cos(\gamma - \theta_{\heartsuit} - \theta_{\spadesuit}) - (\theta_{\heartsuit} - \theta_{\spadesuit}) \cos \gamma] \\
 \Theta_{3,1}(\theta_{\spadesuit}, \theta_{\heartsuit}) & := \frac{1}{2} [\theta_{\heartsuit} - \theta_{\spadesuit} - \sin(\theta_{\heartsuit} - \theta_{\spadesuit}) \cos(\theta_{\heartsuit} + \theta_{\spadesuit})].
 \end{aligned}$$

Due to the above computations, when  $z > 0$  we can conclude that

$$\begin{aligned}
 I_1^{\mathcal{F}} & = \Theta_{1,1}(\theta_{\spadesuit}, \theta_{\heartsuit}) K_{1,1}(\rho_{\clubsuit}, \rho_{\spadesuit}) \quad \text{and} \\
 I_4^{\mathcal{F}} & = \Theta_{1,1}(\theta_{\spadesuit}, \theta_{\heartsuit}) K_{1,3}(\rho_{\clubsuit}, \rho_{\spadesuit})
 \end{aligned}$$

while

$$\begin{aligned}
 I_2^{\mathcal{F}} & = \frac{K_{3,3}(\rho_{\clubsuit}, \rho_{\spadesuit})}{\sin^2 \gamma} [A_{1i} A_{1j} \Theta_{1,3}(\theta_{\spadesuit}, \theta_{\heartsuit}) \\
 & + (A_{1i} A_{2j} + A_{2i} A_{1j}) \Theta_{2,2}(\theta_{\spadesuit}, \theta_{\heartsuit}) \\
 & + A_{2i} A_{2j} \Theta_{3,1}(\theta_{\spadesuit}, \theta_{\heartsuit})] + z \frac{K_{2,3}(\rho_{\clubsuit}, \rho_{\spadesuit})}{\sin \gamma} \\
 & [(A_{1i} A_{3j} + A_{3i} A_{1j}) \Theta_{1,2}(\theta_{\spadesuit}, \theta_{\heartsuit}) \\
 & + (A_{2i} A_{3j} + A_{3i} A_{2j}) \Theta_{2,1}(\theta_{\spadesuit}, \theta_{\heartsuit})] \\
 & + z^2 K_{1,3}(\rho_{\clubsuit}, \rho_{\spadesuit}) \Theta_{1,1}(\theta_{\spadesuit}, \theta_{\heartsuit}) A_{3i} A_{3j}
 \end{aligned}$$

and

$$\begin{aligned}
 I_3^{\mathcal{F}} & = \frac{K_{3,5}(\rho_{\clubsuit}, \rho_{\spadesuit})}{\sin^2 \gamma} \\
 & [A_{1i} A_{1j} \Theta_{1,3}(\theta_{\spadesuit}, \theta_{\heartsuit}) + (A_{1i} A_{2j} + A_{2i} A_{1j}) \Theta_{2,2} \\
 & (\theta_{\spadesuit}, \theta_{\heartsuit}) + A_{2i} A_{2j} \Theta_{3,1}(\theta_{\spadesuit}, \theta_{\heartsuit})] \\
 & + z \frac{K_{2,5}(\rho_{\clubsuit}, \rho_{\spadesuit})}{\sin \gamma} \\
 & [(A_{1i} A_{3j} + A_{3i} A_{1j}) \Theta_{1,2}(\theta_{\spadesuit}, \theta_{\heartsuit}) \\
 & + (A_{2i} A_{3j} + A_{3i} A_{2j}) \Theta_{2,1}(\theta_{\spadesuit}, \theta_{\heartsuit})] \\
 & + z^2 K_{1,5}(\rho_{\clubsuit}, \rho_{\spadesuit}) \Theta_{1,1}(\theta_{\spadesuit}, \theta_{\heartsuit}) A_{3i} A_{3j}.
 \end{aligned}$$

**Remark** In Appendix A we report the values of  $K_{i,j}(0, \rho_{\clubsuit})$  for  $i = j = 1$  or  $i = 1, 2, 3$  and  $j = 3, 5$ . These quantities are useful to compute the integrals over the integration domain  $\mathcal{E}$ .

**Remark** When the field and the source triangles lay on the same plane, i.e.  $z = 0$ , with the help of a limit process that makes  $z$  tending to 0, it is easy to show that

$$I_1^{\mathcal{F}} = \Theta_{1,1}(\theta_{\spadesuit}, \theta_{\heartsuit}) K_1^* \quad \text{and} \quad I_4^{\mathcal{F}} = \Theta_{1,1}(\theta_{\spadesuit}, \theta_{\heartsuit}) K_2^*$$

while

$$\begin{aligned}
 I_2^{\mathcal{F}} & = \frac{K_1^*}{\sin^2 \gamma} [A_{1i} A_{1j} \Theta_{1,3}(\theta_{\spadesuit}, \theta_{\heartsuit}) + (A_{1i} A_{2j} \\
 & + A_{2i} A_{1j}) \Theta_{2,2}(\theta_{\spadesuit}, \theta_{\heartsuit}) + A_{2i} A_{2j} \Theta_{3,1}(\theta_{\spadesuit}, \theta_{\heartsuit})] \\
 I_3^{\mathcal{F}} & = \frac{K_2^*}{\sin^2 \gamma} [A_{1i} A_{1j} \Theta_{1,3}(\theta_{\spadesuit}, \theta_{\heartsuit}) \\
 & + (A_{1i} A_{2j} + A_{2i} A_{1j}) \Theta_{2,2}(\theta_{\spadesuit}, \theta_{\heartsuit}) + A_{2i} A_{2j} \Theta_{3,1}(\theta_{\spadesuit}, \theta_{\heartsuit})],
 \end{aligned}$$

where the constants  $K_1^*$  and  $K_2^*$  following values:

$$K_1^* := (c_P - c_S) \Delta_{n,\tilde{n}} \quad \text{and} \quad K_2^* := \frac{1}{\Delta_{n,\tilde{n}}} \frac{c_P - c_S}{c_P c_S}.$$

### 5.3 Integrals over the region $\mathcal{H}$

If we consider the domain  $\mathcal{D} = \mathcal{H}$  in (5.10) and we use polar coordinates, we obtain double integrals of the type:

$$\begin{aligned}
 & \int_{\theta_{\spadesuit}}^{\theta_{\heartsuit}} (\sin \theta)^{k-1} (\sin(\gamma - \theta))^{h-1} K_{i,j}(\rho_{\clubsuit}, R(\theta)) d\theta \\
 & := \tilde{K}_{i,j}^{k,h}(\rho_{\clubsuit}; \theta_{\spadesuit}, \theta_{\heartsuit}),
 \end{aligned}$$

where the indices  $h, k = 1, 2, 3$  are such that  $2 \leq h + k < 5$ , while the indices  $i$  and  $j$  are such that  $i = j = 1$  or  $i = 1, 2, 3$  and  $j = 3, 5$ . The computation of  $\tilde{K}_{i,j}^{k,h}(\rho_{\clubsuit}; \theta_{\spadesuit}, \theta_{\heartsuit})$  is not

straightforward, since it requires the knowledge of sophisticated relationships linking the complex logarithm to the inverse or hyperbolic sine and cosine, collected in [1]. Furthermore, the results of this computation are given in terms of the following functions:

$$\begin{aligned}
 g_1(\theta_\spadesuit, \theta_\heartsuit) &:= \sqrt{1 + \frac{z^2}{R^2(\theta_\spadesuit)}} \\
 g_2(\theta_\spadesuit, \theta_\heartsuit) &:= \sqrt{1 + \frac{z^2}{R^2(\theta_\heartsuit)}} \\
 g_3(\theta_\spadesuit, \theta_\heartsuit) &:= \frac{1}{2} \log \left( \frac{(g_1(\theta_\spadesuit, \theta_\heartsuit) + \cos(\theta_\spadesuit + \beta))(g_2(\theta_\spadesuit, \theta_\heartsuit) - \cos(\theta_\heartsuit + \beta))}{(g_1(\theta_\spadesuit, \theta_\heartsuit) - \cos(\theta_\spadesuit + \beta))(g_2(\theta_\spadesuit, \theta_\heartsuit) + \cos(\theta_\heartsuit + \beta))} \right) \\
 g_4(\theta_\spadesuit, \theta_\heartsuit) &:= \log \left( \frac{R(\theta_\spadesuit)}{z} + \sqrt{1 + \frac{R^2(\theta_\spadesuit)}{z^2}} \right) \\
 g_5(\theta_\spadesuit, \theta_\heartsuit) &:= \log \left( \frac{R(\theta_\heartsuit)}{z} + \sqrt{1 + \frac{R^2(\theta_\heartsuit)}{z^2}} \right) \\
 g_6(\theta_\spadesuit, \theta_\heartsuit) &:= \pi - \arccos \left( -\frac{z \cos(\theta_\heartsuit + \beta)}{\sqrt{F^2 + z^2}} \right) \\
 &\quad - \arccos \left( \frac{z \cos(\theta_\spadesuit + \beta)}{\sqrt{F^2 + z^2}} \right) \\
 g_7(\theta_\spadesuit, \theta_\heartsuit) &:= \frac{F^2}{F^2 + z^2}.
 \end{aligned}$$

When  $z > 0$ , the analytical integration over the domain  $\mathcal{H}$  yields

$$I_1^{\mathcal{H}} = \tilde{K}_{1,1}^{1,1}(\rho_\clubsuit; \theta_\spadesuit, \theta_\heartsuit) \quad \text{and} \quad I_4^{\mathcal{H}} = \tilde{K}_{1,3}^{1,1}(\rho_\clubsuit; \theta_\spadesuit, \theta_\heartsuit),$$

where

$$\begin{aligned}
 \tilde{K}_{1,1}^{1,1}(\rho_\clubsuit; \theta_\spadesuit, \theta_\heartsuit) &:= F g_3(\theta_\spadesuit, \theta_\heartsuit) + z g_6(\theta_\spadesuit, \theta_\heartsuit) - (\theta_\heartsuit - \theta_\spadesuit) \sqrt{\rho_\clubsuit^2 + z^2} \\
 \tilde{K}_{1,3}^{1,1}(\rho_\clubsuit; \theta_\spadesuit, \theta_\heartsuit) &:= -\frac{1}{z} g_6(\theta_\spadesuit, \theta_\heartsuit) + \frac{\theta_\heartsuit - \theta_\spadesuit}{\sqrt{\rho_\clubsuit^2 + z^2}}.
 \end{aligned}$$

For what concerns the computation of  $I_2^{\mathcal{H}}$ , we have:

$$\begin{aligned}
 I_2^{\mathcal{H}} &= \frac{1}{\sin^2 \gamma} \left[ A_{1i} A_{1j} \tilde{K}_{3,3}^{1,3}(\rho_\clubsuit; \theta_\spadesuit, \theta_\heartsuit) + (A_{1i} A_{2j} + A_{2i} A_{1j}) \right. \\
 &\quad \left. \tilde{K}_{3,3}^{2,2}(\rho_\clubsuit; \theta_\spadesuit, \theta_\heartsuit) + A_{2i} A_{2j} \tilde{K}_{3,3}^{3,1}(\rho_\clubsuit; \theta_\spadesuit, \theta_\heartsuit) \right] \\
 &+ \frac{z}{\sin \gamma} \left[ (A_{1i} A_{3j} + A_{3i} A_{1j}) \tilde{K}_{2,3}^{1,2}(\rho_\clubsuit; \theta_\spadesuit, \theta_\heartsuit) \right. \\
 &\quad \left. + (A_{2i} A_{3j} + A_{3i} A_{2j}) \tilde{K}_{2,3}^{2,1}(\rho_\clubsuit; \theta_\spadesuit, \theta_\heartsuit) \right] \\
 &+ z^2 A_{3i} A_{3j} \tilde{K}_{1,3}^{1,1}(\rho_\clubsuit; \theta_\spadesuit, \theta_\heartsuit),
 \end{aligned}$$

where:

$$\begin{aligned}
 \tilde{K}_{2,3}^{1,2}(\rho_\clubsuit; \theta_\spadesuit, \theta_\heartsuit) &:= g_5(\theta_\spadesuit, \theta_\heartsuit) \cos(\gamma - \theta_\heartsuit) \\
 &\quad - g_4(\theta_\spadesuit, \theta_\heartsuit) \cos(\gamma - \theta_\spadesuit) - g_3(\theta_\spadesuit, \theta_\heartsuit) \cos \alpha
 \end{aligned}$$

$$+ \left[ \frac{\rho_\clubsuit}{\sqrt{\rho_\clubsuit^2 + z^2}} - \log \left( \frac{\rho_\clubsuit + \sqrt{\rho_\clubsuit^2 + z^2}}{z} \right) \right]$$

$$[\cos(\gamma - \theta_\heartsuit) - \cos(\gamma - \theta_\spadesuit)]$$

$$\tilde{K}_{2,3}^{2,1}(\rho_\clubsuit; \theta_\spadesuit, \theta_\heartsuit) := -g_5(\theta_\spadesuit, \theta_\heartsuit) \cos \theta_\heartsuit$$

$$+ g_4(\theta_\spadesuit, \theta_\heartsuit) \cos \theta_\spadesuit - g_3(\theta_\spadesuit, \theta_\heartsuit) \cos \beta$$

$$- \left[ \frac{\rho_\clubsuit}{\sqrt{\rho_\clubsuit^2 + z^2}} - \log \left( \frac{\rho_\clubsuit + \sqrt{\rho_\clubsuit^2 + z^2}}{z} \right) \right] (\cos \theta_\heartsuit - \cos \theta_\spadesuit)$$

$$\tilde{K}_{3,3}^{1,3}(\rho_\clubsuit; \theta_\spadesuit, \theta_\heartsuit) := F [g_2(\theta_\spadesuit, \theta_\heartsuit) \cos(\theta_\heartsuit + \alpha - \gamma)$$

$$- g_1(\theta_\spadesuit, \theta_\heartsuit) \cos(\theta_\spadesuit + \alpha - \gamma) + g_3(\theta_\spadesuit, \theta_\heartsuit) \sin^2 \alpha]$$

$$+ z g_6(\theta_\spadesuit, \theta_\heartsuit) - \frac{\rho_\clubsuit^2 + 2z^2}{\sqrt{\rho_\clubsuit^2 + z^2}} \Theta_{1,3}(\theta_\spadesuit, \theta_\heartsuit)$$

$$\tilde{K}_{3,3}^{2,2}(\rho_\clubsuit; \theta_\spadesuit, \theta_\heartsuit) := F [g_1(\theta_\spadesuit, \theta_\heartsuit) \cos(\theta_\spadesuit + \alpha) - g_2(\theta_\spadesuit, \theta_\heartsuit)$$

$$\cos(\theta_\heartsuit + \alpha) - g_3(\theta_\spadesuit, \theta_\heartsuit) \sin \alpha \sin \beta]$$

$$- z g_6(\theta_\spadesuit, \theta_\heartsuit) \cos \gamma - \frac{\rho_\clubsuit^2 + 2z^2}{\sqrt{\rho_\clubsuit^2 + z^2}} \Theta_{2,2}(\theta_\spadesuit, \theta_\heartsuit)$$

$$\tilde{K}_{3,3}^{3,1}(\rho_\clubsuit; \theta_\spadesuit, \theta_\heartsuit) := F [g_1(\theta_\spadesuit, \theta_\heartsuit) \cos(\theta_\spadesuit - \beta)$$

$$- g_2(\theta_\spadesuit, \theta_\heartsuit) \cos(\theta_\heartsuit - \beta) + g_3(\theta_\spadesuit, \theta_\heartsuit) \sin^2 \beta]$$

$$+ z g_6(\theta_\spadesuit, \theta_\heartsuit) - \frac{\rho_\clubsuit^2 + 2z^2}{\sqrt{\rho_\clubsuit^2 + z^2}} \Theta_{3,1}(\theta_\spadesuit, \theta_\heartsuit).$$

Finally,

$$\begin{aligned}
 I_3^{\mathcal{H}} &= \frac{1}{\sin^2 \gamma} \left[ A_{1i} A_{1j} \tilde{K}_{3,5}^{1,3}(\rho_\clubsuit; \theta_\spadesuit, \theta_\heartsuit) \right. \\
 &\quad \left. + (A_{1i} A_{2j} + A_{2i} A_{1j}) \tilde{K}_{3,5}^{2,2}(\rho_\clubsuit; \theta_\spadesuit, \theta_\heartsuit) \right. \\
 &\quad \left. + A_{2i} A_{2j} \tilde{K}_{3,5}^{3,1}(\rho_\clubsuit; \theta_\spadesuit, \theta_\heartsuit) \right] \\
 &+ \frac{z}{\sin \gamma} \left[ (A_{1i} A_{3j} + A_{3i} A_{1j}) \tilde{K}_{2,5}^{1,2}(\rho_\clubsuit; \theta_\spadesuit, \theta_\heartsuit) \right. \\
 &\quad \left. + (A_{2i} A_{3j} + A_{3i} A_{2j}) \tilde{K}_{2,5}^{2,1}(\rho_\clubsuit; \theta_\spadesuit, \theta_\heartsuit) \right] \\
 &+ z^2 A_{3i} A_{3j} \tilde{K}_{1,5}^{1,1}(\rho_\clubsuit; \theta_\spadesuit, \theta_\heartsuit).
 \end{aligned}$$

where

$$\tilde{K}_{1,5}^{1,1}(\rho_\clubsuit; \theta_\spadesuit, \theta_\heartsuit) := -\frac{1}{3z^2} \frac{F}{F^2 + z^2}$$

$$\left[ \frac{\cos(\theta_\heartsuit + \beta)}{g_2(\theta_\spadesuit, \theta_\heartsuit)} - \frac{\cos(\theta_\spadesuit + \beta)}{g_1(\theta_\spadesuit, \theta_\heartsuit)} \right]$$

$$- \frac{g_6(\theta_\spadesuit, \theta_\heartsuit)}{3z^3} + \frac{\theta_\heartsuit - \theta_\spadesuit}{3(\rho_\clubsuit^2 + z^2)^{3/2}}$$

$$\tilde{K}_{2,5}^{1,2}(\rho_\clubsuit; \theta_\spadesuit, \theta_\heartsuit) := -\frac{\rho_\clubsuit^3}{3z^2(\rho_\clubsuit^2 + z^2)^{3/2}} \Theta_{1,2}(\theta_\spadesuit, \theta_\heartsuit)$$

$$+ \frac{1}{3z^2} \left[ \frac{\sin \alpha \sin(\theta_\heartsuit + \beta) - g_7(\theta_\spadesuit, \theta_\heartsuit) \cos \alpha \cos(\theta_\heartsuit + \beta)}{g_2(\theta_\spadesuit, \theta_\heartsuit)} \right]$$

$$\begin{aligned}
 & + \frac{g_7(\theta_\diamond, \theta_\heartsuit) \cos \alpha \cos(\theta_\diamond + \beta) - \sin \alpha \sin(\theta_\diamond + \beta)}{g_1(\theta_\diamond, \theta_\heartsuit)} \Big] \\
 \tilde{K}_{2,5}^{2,1}(\rho_\clubsuit; \theta_\diamond, \theta_\heartsuit) & := -\frac{\rho_\clubsuit^3}{3z^2(\rho_\clubsuit^2 + z^2)^{3/2}} \Theta_{2,1}(\theta_\diamond, \theta_\heartsuit) \\
 & + \frac{1}{3z^2} \left[ \frac{\sin \beta \sin(\theta_\diamond + \beta) + g_7(\theta_\diamond, \theta_\heartsuit) \cos \beta \cos(\theta_\diamond + \beta)}{g_1(\theta_\diamond, \theta_\heartsuit)} + \right. \\
 & \left. - \frac{\sin \beta \sin(\theta_\heartsuit + \beta) + g_7(\theta_\diamond, \theta_\heartsuit) \cos \beta \cos(\theta_\heartsuit + \beta)}{g_2(\theta_\diamond, \theta_\heartsuit)} \right] \\
 \tilde{K}_{3,5}^{1,3}(\rho_\clubsuit; \theta_\diamond, \theta_\heartsuit) & := \frac{3\rho_\clubsuit^2 + 2z^2}{3(\rho_\clubsuit^2 + z^2)^{3/2}} \Theta_{1,3}(\theta_\diamond, \theta_\heartsuit) \\
 & - \frac{g_6(\theta_\diamond, \theta_\heartsuit)}{3z} \\
 & + \frac{g_7(\theta_\diamond, \theta_\heartsuit) \cos^2 \alpha \cos(\theta_\heartsuit + \beta) - \cos(\theta_\heartsuit + \alpha - \gamma) \sin^2(\theta_\heartsuit + \beta)}{3Fg_2(\theta_\diamond, \theta_\heartsuit)} \\
 & - \frac{g_7(\theta_\diamond, \theta_\heartsuit) \cos^2 \alpha \cos(\theta_\diamond + \beta) - \cos(\theta_\diamond + \alpha - \gamma) \sin^2(\theta_\diamond + \beta)}{3Fg_1(\theta_\diamond, \theta_\heartsuit)} \\
 \tilde{K}_{3,5}^{2,2}(\rho_\clubsuit; \theta_\diamond, \theta_\heartsuit) & := \frac{3\rho_\clubsuit^2 + 2z^2}{3(\rho_\clubsuit^2 + z^2)^{3/2}} \Theta_{2,2}(\theta_\diamond, \theta_\heartsuit) \\
 & + \frac{g_6(\theta_\diamond, \theta_\heartsuit)}{3z} \cos \gamma \\
 & + \frac{g_7(\theta_\diamond, \theta_\heartsuit) \cos \alpha \cos \beta \cos(\theta_\heartsuit + \beta) + \cos(\theta_\heartsuit + \alpha) \sin^2(\theta_\heartsuit + \beta)}{3Fg_2(\theta_\diamond, \theta_\heartsuit)} \\
 & - \frac{g_7(\theta_\diamond, \theta_\heartsuit) \cos \alpha \cos \beta \cos(\theta_\diamond + \beta) + \cos(\theta_\diamond + \alpha) \sin^2(\theta_\diamond + \beta)}{3Fg_1(\theta_\diamond, \theta_\heartsuit)} \\
 \tilde{K}_{3,5}^{3,1}(\rho_\clubsuit; \theta_\diamond, \theta_\heartsuit) & := \frac{3\rho_\clubsuit^2 + 2z^2}{3(\rho_\clubsuit^2 + z^2)^{3/2}} \Theta_{3,1}(\theta_\diamond, \theta_\heartsuit) - \frac{g_6(\theta_\diamond, \theta_\heartsuit)}{3z} \\
 & + \frac{g_7(\theta_\diamond, \theta_\heartsuit) \cos^2 \beta \cos(\theta_\heartsuit + \beta) + \cos(\theta_\heartsuit - \beta) \sin^2(\theta_\heartsuit + \beta)}{3Fg_2(\theta_\diamond, \theta_\heartsuit)} \\
 & - \frac{g_7(\theta_\diamond, \theta_\heartsuit) \cos^2 \beta \cos(\theta_\diamond + \beta) + \cos(\theta_\diamond - \beta) \sin^2(\theta_\diamond + \beta)}{3Fg_1(\theta_\diamond, \theta_\heartsuit)}.
 \end{aligned}$$

**Remark** The values  $\tilde{K}_{i,j}^{h,k}(\theta_\diamond, \theta_\heartsuit) := \tilde{K}_{i,j}^{h,k}(0; \theta_\diamond, \theta_\heartsuit)$ , for  $i = j = 1$  or  $i = 1, 2, 3$  and  $j = 3, 5$ , are collected in Appendix B. We point out that these functions are involved in the computation of the integral over the domain  $\mathcal{G}$ .

**Remark** When the source and the field triangles are in the same plane, i.e.  $z = 0$ , we introduce the function

$$g(\theta_\diamond, \theta_\heartsuit) := \frac{1}{2} \log \left( \frac{(1 + \cos(\theta_\diamond + \beta))(1 - \cos(\theta_\heartsuit + \beta))}{(1 - \cos(\theta_\diamond + \beta))(1 + \cos(\theta_\heartsuit + \beta))} \right)$$

and we consider:

$$I_1^{\mathcal{H}} = \bar{K}_{1,1}^{1,1}(\rho_\clubsuit; \theta_\diamond, \theta_\heartsuit) \quad \text{and} \quad I_4^{\mathcal{H}} = \bar{K}_{1,3}^{1,1}(\rho_\clubsuit; \theta_\diamond, \theta_\heartsuit),$$

where

$$\begin{aligned}
 \bar{K}_{1,1}^{1,1}(\rho_\clubsuit; \theta_\diamond, \theta_\heartsuit) & := Fg(\theta_\diamond, \theta_\heartsuit) - \rho_\clubsuit(\theta_\heartsuit - \theta_\diamond) \\
 \bar{K}_{1,3}^{1,1}(\rho_\clubsuit; \theta_\diamond, \theta_\heartsuit) & := \frac{1}{F} [\cos(\theta_\heartsuit + \beta) - \cos(\theta_\diamond + \beta)] + \frac{\theta_\heartsuit - \theta_\diamond}{\rho_\clubsuit}.
 \end{aligned}$$

The value of  $I_2^{\mathcal{H}}$  is given by the following relationship:

$$\begin{aligned}
 I_2^{\mathcal{H}} & = \frac{1}{\sin^2 \gamma} \left[ A_{1i} A_{1j} \bar{K}_{3,3}^{1,3}(\rho_\clubsuit; \theta_\diamond, \theta_\heartsuit) \right. \\
 & \quad + (A_{1i} A_{2j} + A_{2i} A_{1j}) \bar{K}_{3,3}^{2,2}(\rho_\clubsuit; \theta_\diamond, \theta_\heartsuit) \\
 & \quad \left. + A_{2i} A_{2j} \bar{K}_{3,3}^{3,1}(\rho_\clubsuit; \theta_\diamond, \theta_\heartsuit) \right]
 \end{aligned}$$

where

$$\begin{aligned}
 \bar{K}_{3,3}^{1,3}(\rho_\clubsuit; \theta_\diamond, \theta_\heartsuit) & := F[g(\theta_\diamond, \theta_\heartsuit) \sin^2 \alpha + \cos(\theta_\heartsuit + \alpha - \gamma) \\
 & \quad - \cos(\theta_\diamond + \alpha - \gamma)] \\
 & \quad - \rho_\clubsuit \Theta_{1,3}(\theta_\diamond, \theta_\heartsuit) \\
 \bar{K}_{3,3}^{2,2}(\rho_\clubsuit; \theta_\diamond, \theta_\heartsuit) & := F[\cos(\theta_\diamond + \alpha) - \cos(\theta_\heartsuit + \alpha) - g(\theta_\diamond, \theta_\heartsuit) \sin \alpha \sin \beta] \\
 & \quad - \rho_\clubsuit \Theta_{2,2}(\theta_\diamond, \theta_\heartsuit) \\
 \bar{K}_{3,3}^{3,1}(\rho_\clubsuit; \theta_\diamond, \theta_\heartsuit) & := F[\cos(\theta_\diamond - \beta) - \cos(\theta_\heartsuit - \beta) \\
 & \quad + g(\theta_\diamond, \theta_\heartsuit) \sin^2 \beta] \\
 & \quad - \rho_\clubsuit \Theta_{3,1}(\theta_\diamond, \theta_\heartsuit).
 \end{aligned}$$

Finally, the computation of  $I_3^{\mathcal{H}}$  yields

$$\begin{aligned}
 I_3^{\mathcal{H}} & = \frac{1}{\sin^2 \gamma} \\
 & \quad \left[ A_{1i} A_{1j} \bar{K}_{3,5}^{1,3}(\rho_\clubsuit; \theta_\diamond, \theta_\heartsuit) + (A_{1i} A_{2j} + A_{2i} A_{1j}) \bar{K}_{3,5}^{2,2}(\rho_\clubsuit; \theta_\diamond, \theta_\heartsuit) \right. \\
 & \quad \left. + A_{2i} A_{2j} \bar{K}_{3,5}^{3,1}(\rho_\clubsuit; \theta_\diamond, \theta_\heartsuit) \right]
 \end{aligned}$$

700 where  
701

$$\begin{aligned} \overline{K}_{3,5}^{1,3}(\rho_{\clubsuit}; \theta_{\spadesuit}, \theta_{\heartsuit}) &:= \frac{(1 + \cos^2 \alpha) \cos(\theta_{\heartsuit} + \beta) - \cos(\theta_{\heartsuit} + \alpha - \gamma) \sin^2(\theta_{\heartsuit} + \beta)}{3F} \\ &- \frac{(1 + \cos^2 \alpha) \cos(\theta_{\spadesuit} + \beta) - \cos(\theta_{\spadesuit} + \alpha - \gamma) \sin^2(\theta_{\spadesuit} + \beta)}{3F} \\ &+ \frac{1}{\rho_{\clubsuit}} \Theta_{1,3}(\theta_{\spadesuit}, \theta_{\heartsuit}) \overline{K}_{3,5}^{2,2}(\rho_{\clubsuit}; \theta_{\spadesuit}, \theta_{\heartsuit}) := \frac{[\cos \alpha \cos \beta + \cos(\alpha + \beta)] \cos(\theta_{\heartsuit} + \beta) + \cos(\theta_{\heartsuit} + \alpha) \sin^2(\theta_{\heartsuit} + \beta)}{3F} \\ &- \frac{[\cos \alpha \cos \beta + \cos(\alpha + \beta)] \cos(\theta_{\spadesuit} + \beta) + \cos(\theta_{\spadesuit} + \alpha) \sin^2(\theta_{\spadesuit} + \beta)}{3F} + \frac{1}{\rho_{\clubsuit}} \Theta_{2,2}(\theta_{\spadesuit}, \theta_{\heartsuit}) \overline{K}_{3,5}^{3,1}(\rho_{\clubsuit}; \theta_{\spadesuit}, \theta_{\heartsuit}) \\ &:= \frac{(1 + \cos^2 \beta) \cos(\theta_{\heartsuit} + \beta) + \cos(\theta_{\heartsuit} - \beta) \sin^2(\theta_{\heartsuit} + \beta)}{3F} - \frac{(1 + \cos^2 \beta) \cos(\theta_{\spadesuit} + \beta) + \cos(\theta_{\spadesuit} - \beta) \sin^2(\theta_{\spadesuit} + \beta)}{3F} \\ &+ \frac{1}{\rho_{\clubsuit}} \Theta_{3,1}(\theta_{\spadesuit}, \theta_{\heartsuit}). \end{aligned}$$

702 **6 Numerical results**

703 Here, we address three numerical examples to validate the  
704 EBEM approach. As recalled in the previous section, double  
705 time integrals are performed analytically as well as the  
706 inner space integral over the field triangle. On the contrary,  
707 the outer space integral over the source element is numerically  
708 computed by using  $M_g$ -point Gauss-Hammer quadrature rules.  
709 The choice of the parameter  $M_g \leq 12$  has guaranteed the  
710 computation of all the involved integrals with a sufficiently high  
711 accuracy. Higher values of  $M_g$  could be considered, but they  
712 would increase the overall computational cost of the method.

714 For the generation of the partitioning  $\mathcal{T}_{\Delta_x}(\Gamma)$ , we have  
715 used the GMSH software (see [22]). In particular, we have built  
716 uniform or quasi-uniform conforming meshes consisting of  
717 triangular elements. All the numerical computations have been  
718 performed on a cluster with two Intel® XEON® E5-2683v4  
719 CPUs (2.1 GHz clock frequency and 16 cores) by means of  
720 parallel MATLAB® codes.

721 **6.1 Error analysis for an elastodynamic problem exterior to a square crack**

723 In this example, we consider a square crack  $\Gamma = \{\mathbf{x} = (x_1, x_2, 0) : -0.5 \leq x_i \leq 0.5, i = 1, 2\}$  and the elastodynamic problem defined in  $\Omega = \mathbf{R}^3 \setminus \Gamma$ , equipped by Dirichlet boundary conditions given on  $\Gamma$ . The chosen P, S-velocities are  $c_P = 1^{m/s}$  and  $c_S = 1/\sqrt{2}^{m/s}$ , the material density is  $\rho = 1^{kg/m^3}$  and the final time is  $T = 1s$ . The boundary datum  $\mathbf{g}(\mathbf{x}; t)$  is assigned in such a way that the analytical solution of (3.9) turns out to be  $\mathbf{w}(\mathbf{x}; t) = \mathbf{x}t$ . We consider successive refinements levels of a uniform coarse

731 mesh constituted by 8 equal triangles (lev. 0) covering  $\Gamma$ .  
732 Refinements are obtained halving each triangle side, giving  
733 meshes as those depicted in Fig.6. In Table 1 we show the  
734 discretization parameters, together with the error evaluated  
735 in  $L^2(\Gamma \times [0, T])$  norm:  
736

$$\begin{aligned} \varepsilon_{L^2(\Gamma \times [0, T])} &:= \|\mathbf{w} - \tilde{\mathbf{w}}\|_{L^2(\Gamma \times [0, T])} \\ &= \left[ \int_{\Gamma} \int_0^T \|\mathbf{w}(\mathbf{x}; t) - \tilde{\mathbf{w}}(\mathbf{x}; t)\|^2 d\Gamma_{\mathbf{x}} dt \right]^{1/2} \end{aligned}$$

737 and the Estimated Order of Convergence (EOC). We remark  
738 that, here,  $\Delta_x$  corresponds to the cathetus length of the uniform  
739 mesh elements, while  $\Delta_t$  has been chosen in a way such that  
740  $c_P = \frac{\Delta_x}{\Delta_t}$ .  
741

742 As one can see, the error decays as  $O(\Delta_x^{1.5})$ . The observed  
743 super-convergence could be ascribed to the regularity of the  
744 meshes and the smoothness of the solution.  
745

746 **6.2 Longitudinal waves in a bar**

747 To study the behaviour of the proposed method, we will deduce a  
748 Dirichlet problem from a classical benchmark for

**Table 1** Discretization parameters for different levels of refinement, space-time  $L^2$  error and EOC

	$\Delta_x = c_P \Delta_t$	$M_{\Delta_x}$	$N_{\Delta_t}$	$\varepsilon_{L^2(\Gamma \times [0, T])}$	EOC
lev. 0	0.50000	8	2	$4.20 \cdot 10^{-2}$	–
lev. 1	0.25000	32	4	$1.52 \cdot 10^{-2}$	1.47
lev. 2	0.12500	128	8	$5.21 \cdot 10^{-3}$	1.54
lev. 3	0.06250	512	16	$1.81 \cdot 10^{-3}$	1.52
lev. 4	0.03125	2048	32	$6.65 \cdot 10^{-4}$	1.45

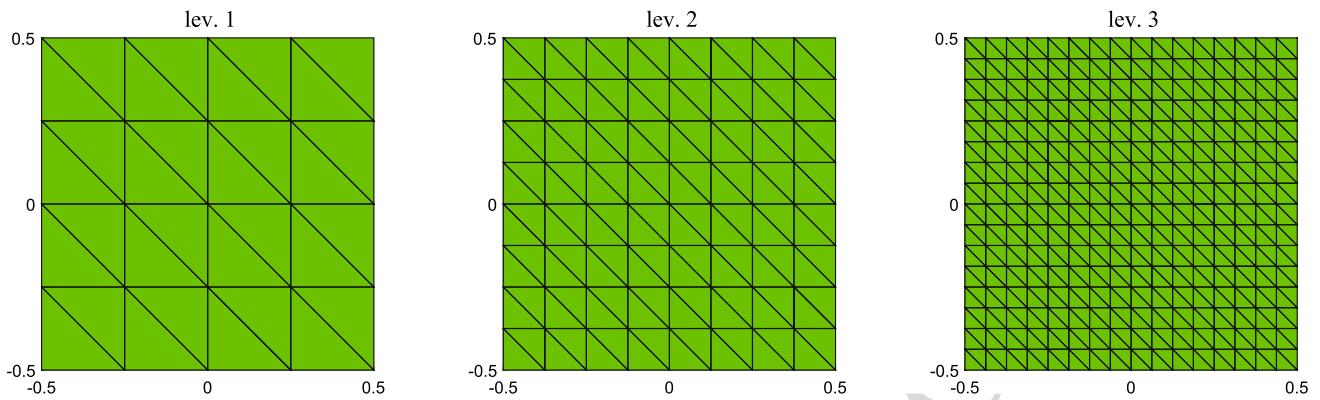


Fig. 6 Meshes on the square crack for successive refinement levels

749 time-domain BEMs applied to 3D elastodynamics, which is  
 750 well known to be extremely challenging for what concern  
 751 standard BEMs analysis in terms of stability properties.

752 Let us consider a bar  $\Omega_i$  of height equal to  $L$  and square  
 753 cross section with unit side, depicted in Fig. 7. In litera-  
 754 ture, this domain is typically equipped with mixed boundary  
 755 conditions: on the lower surface the Dirichlet boundary  
 756 datum  $\bar{\mathbf{u}}(\mathbf{x}; t) = (0, 0, 0)^\top$  is enforced, while the upper sur-  
 757 face is subjected to a uniform normal traction  $\bar{\mathbf{p}}(\mathbf{x}; t) =$   
 758  $(0, 0, p_0 H(t))^\top$ . On the remaining boundary the tractions  
 759 are set to zero.

760 If we set a (artificially) vanishing Poisson’s ratio and, con-  
 761 sequently  $c_P = \sqrt{2}c_S$ , the related elastodynamic problem  
 762 possesses an analytical solution, representing the total dis-  
 763 placement field in the whole 3D bar volume and surface,  
 764 directed only in  $x_3$ -direction and whose expression coincides  
 765 with that of the longitudinal waves in a 1D elastodynamic rod  
 766 (see [21], page 473), i.e.:

$$\begin{aligned}
 u(x; t) = & \frac{p_0 H(t)}{\rho c_P^2} \sum_{k=0}^{\lceil \frac{c_P t}{2L} \rceil - 1} (-1)^k \\
 & \left[ (c_P t - 2kL - (L - x)) \right. \\
 & H\left(\frac{c_P t - 2kL - (L - x)}{c_P}\right) \\
 & - (c_P t - 2(k + 1)L + (L - x)) \\
 & \left. \times H\left(\frac{c_P t - 2(k + 1)L + (L - x)}{c_P}\right) \right], \tag{6.1}
 \end{aligned}$$

768 Here, we consider problem (2.1), where  $\Omega_i = [-l, l]^2 \times$   
 769  $[0, L]$ , with  $l = \frac{1}{2}m$ ,  $L = 3m$ . The material parameters  
 770  $\rho = 1 \text{ kg/m}^3$  and  $\mu = \frac{1}{2} \text{ kg/ms}^2$  are taken, while we set  $p_0 =$   
 771  $1 \text{ kg/ms}^2$ , so that  $p_0/\rho c_P^2 = 1$ . Using (6.1), on the boundary  $\Gamma$   
 772 of the bar we prescribe the Dirichlet condition:

$$\mathbf{g}(\mathbf{x}; t) = (0, 0, u(x_3; t))^\top, \quad \mathbf{x} \in \Gamma, t \in [0, T] \tag{6.2}$$

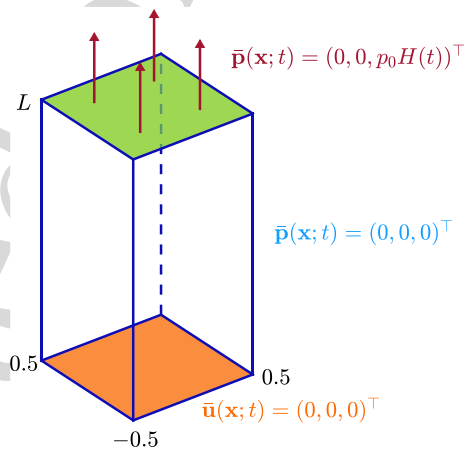


Fig. 7 Bar geometry and boundary conditions typically prescribed in literature

774 where the overall analyzed time is  $T = 36s$ . To develop  
 775 a convergence analysis, we start by considering the coarse  
 776 mesh associated to the zero level of refinement (lev. 0) and all  
 777 the successive refinements are obtained by halving each side  
 778 of its elements. In Fig. 8, the uniform meshes corresponding  
 779 to the four levels of refinement are represented. In Table 2,  
 780 the space and time discretization parameters are reported. We  
 781 remark that, here,  $\Delta_x$  corresponds to the cathetus length of the  
 782 uniform mesh elements, while  $\Delta_t$  has been chosen in a way  
 783 such that  $c_P = \frac{\Delta_x}{\Delta_t}$ . Furthermore, the last column of Table 2  
 784 collects the values of the parameter  $N^*$  in (4.11), responsible  
 785 for the reduction of the cost of the proposed approach in  
 786 terms of memory and computation time. Indeed, we recall  
 787 that  $\mathbb{E}^{(\ell)} = 0$  for  $\ell = N^*, \dots, N_{\Delta_t} - 1$ .

788 In Fig. 9, we show in relation to the finest mesh the whole  
 789 time history of the third component of the recovered density  
 790  $\tilde{w}_3(\mathbf{x}; t)$  at the points  $\mathbf{x}_0 = (0, 0, 0)$  (on the bottom face) and  
 791  $\mathbf{x}_6 = (0, 0, 3)$  (on the top face), since the components in the  
 792  $x_1$ - and  $x_2$ -directions of the density  $\tilde{\mathbf{w}}(\mathbf{x}; t)$  are both trivial.  
 793 We remark that the oscillations in these plots are clearly asso-

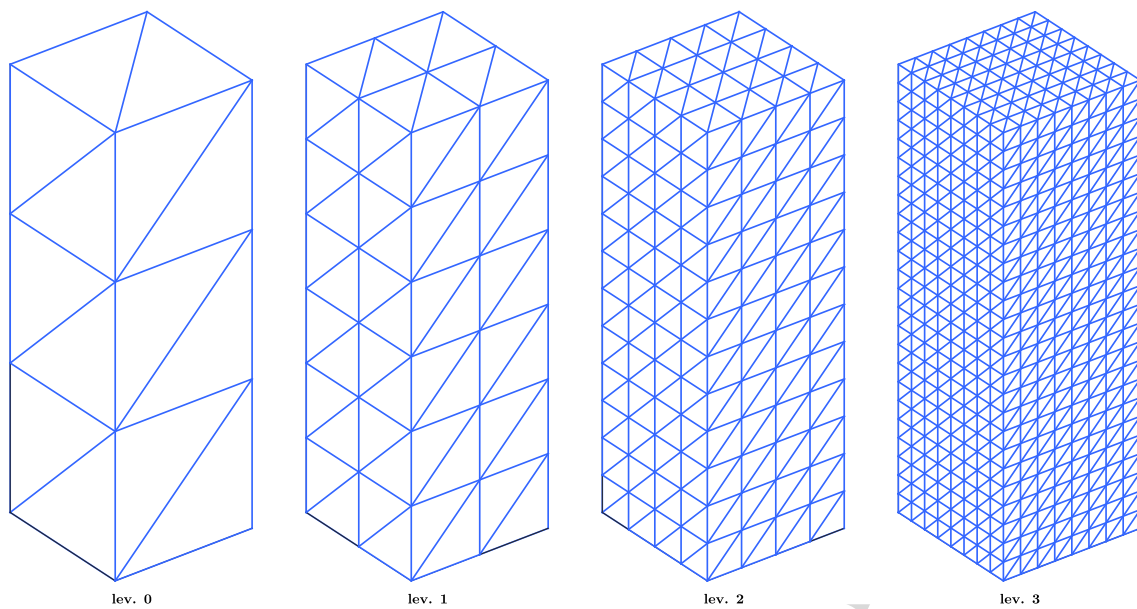


Fig. 8 Meshes of the domain  $\Omega_i$  for four successive levels of refinement

Table 2 Discretization parameters for different levels of refinement of the bar boundary mesh

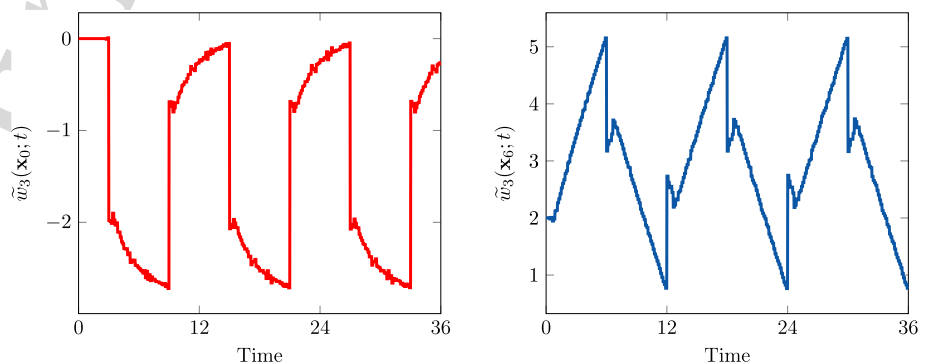
	$\Delta_x$	$M_{\Delta_x}$	$\Delta_t$	$N_{\Delta_t}$	$N^*$
lev. 0	1.0000	28	1.0000	36	10
lev. 1	0.5000	112	0.5000	72	14
lev. 2	0.2500	448	0.2500	144	24
lev. 3	0.1250	1792	0.1250	288	42

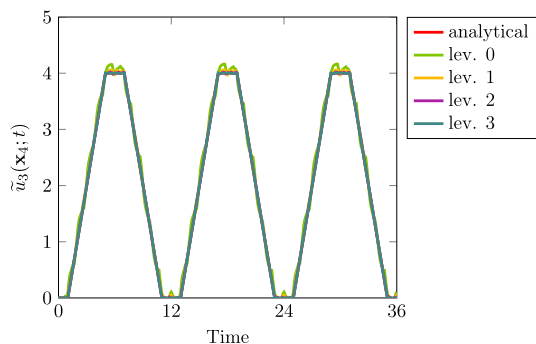
shown in Fig. 10, where for the highest levels of refinement the recovered displacement  $\tilde{\mathbf{u}}$  in  $\mathbf{x}_4 = (0, 0, 2)$  is indistinguishable from the exact one. This good approximation property is clearly visible also in Fig. 11, where only for  $\Delta_x = \Delta_t = 0.125$ , the picture on the left presents the whole time history of the recovered displacement field, computed at one of the points, namely  $\mathbf{x}_6$ , of the upper surface compared to the exact one, while on the right, the behaviour of  $\tilde{u}_3$  at the points  $\mathbf{x}_j = (0, 0, j/2)$ , for  $j = 0, 1, 2, 3, 4, 5, 6$  (placed along a vertical line in the center of the bar) is highlighted. In order to test the accuracy of the numerical solution retrieved by applying the proposed energetic BEM approach, in Fig. 12, we show the behaviour of the  $L^2([0, T])$  absolute error in the point  $\mathbf{x}_4$ :

$$\begin{aligned} \varepsilon(\mathbf{x}_4) &:= \|\tilde{u}_3(\mathbf{x}_4; \cdot) - u(2; \cdot)\|_{L^2([0, T])} \\ &= \sqrt{\int_0^T |\tilde{u}_3(\mathbf{x}_4; t) - u(2; t)|^2 dt}. \end{aligned}$$

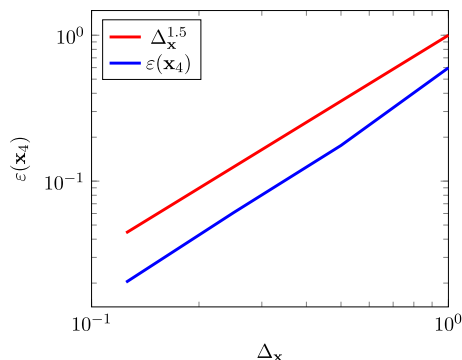
794 ciated with the jump discontinuities of the analytical solution,  
 795 but anyway they remain stable.  
 796 To reconstruct the solution of the elastodynamic problem  
 797  $\mathbf{u}(\mathbf{x}; t) = (0, 0, u(x_3; t))$ ,  $\mathbf{x} \in \Omega_i$ , we plug the computed  
 798 density  $\tilde{\mathbf{w}}(\mathbf{x}; t)$  into the relationship (3.1), obtaining  $\tilde{\mathbf{u}}(\mathbf{x}; t)$ .  
 799 The analytical behaviour of the time history of  $\mathbf{u}$  is well  
 800 captured by the third component of  $\tilde{\mathbf{u}}$  (the only one not  
 801 trivial) for every choice of  $\Delta_x, \Delta_t$  presented in Table 2, in  
 802 particular for the smallest discretization parameters, as it is

Fig. 9 For  $\Delta_t = 0.125$ , time history of the component in  $x_3$ -direction of the approximated density  $\tilde{\mathbf{w}}$  at the location  $\mathbf{x}_0 = (0, 0, 0)$ , on the left, and  $\mathbf{x}_6 = (0, 0, 3)$ , on the right





**Fig. 10** Time history of the component in  $x_3$ -direction of the approximated displacement field  $\tilde{\mathbf{u}}$  in  $\mathbf{x}_4 = (0, 0, 2)$ , recovered for different values of discretization parameters and compared to the analytical one



**Fig. 12**  $L^2([0, T])$  absolute error  $\varepsilon(\mathbf{x}_4)$  for the sequence of time and space discretizations described in Table 2

819 We point out that these results seem to suggest that  $\varepsilon(\mathbf{x}_4)$   
 820 decays as  $O(\Delta_x^{1.5})$ . In our numerical experiments, we have  
 821 observed similar errors when we reconstruct  $\tilde{\mathbf{u}}(\mathbf{x}; t)$  in other  
 822 points  $\mathbf{x} \in \Omega_i$ .

823 **6.3 Scattering of an incident plane P-wave by the**  
 824 **unit sphere**

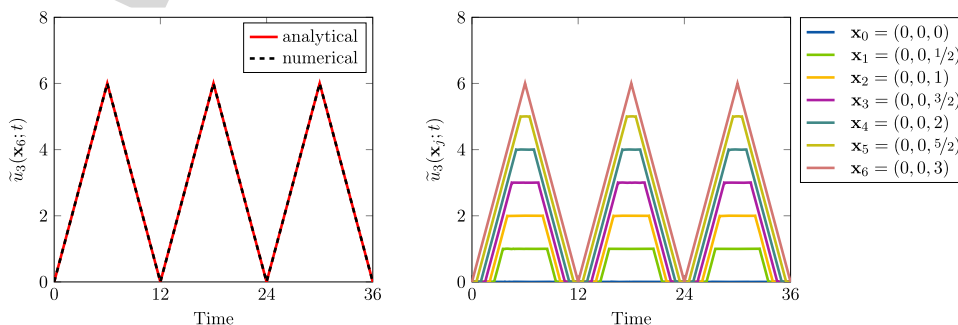
825 Finally, we consider the problem of scattering by a sphere,  
 826 which is interesting from the mathematical point of view and  
 827 has several applications, as reviewed in [30], ranging from  
 828 acoustics to elastodynamics (see also [32]) and electromag-  
 829 netism.

830 Problem (2.1) is here defined in the domain  $\Omega_e := \{\mathbf{x} \in$   
 831  $\mathbf{R}^3 \mid x_1^2 + x_2^2 + x_3^2 > 1\}$ , external to the unit sphere with  
 832 boundary  $\Gamma$  and centered at the origin of the axes, endowed  
 833 with homogeneous initial data and Dirichlet datum  $\mathbf{g}(\mathbf{x}; t)$   
 834 coinciding with the opposite of an incident plane P-wave  
 835  $\mathbf{u}_{\text{inc}}(\mathbf{x}; t)$  along the obstacle  $\Gamma$ , i.e.  $\mathbf{g}(\mathbf{x}; t) = -\mathbf{u}_{\text{inc}}(\mathbf{x}; t)$ . In  
 836 the following, we assume:

837  $\mathbf{u}_{\text{inc}}(\mathbf{x}; t)$   
 838  $:= \left( e^{-20(x_1 - 2 + c_P t - 0.475)^2}, 0, 0 \right)^T$ .

839 The chosen P, S-velocities are  $c_P = 2^{m/s}$  and  $c_S = 1^{m/s}$ , the  
 840 material density is  $\rho = 1^{kg/m^3}$  and the final time is  $T = 12s$ .

**Fig. 11** For  $\Delta_x = 0.125$ ,  $\Delta_t = 0.125$ , on the left, time history of the component in  $x_3$ -direction of the recovered displacement field  $\tilde{\mathbf{u}}$  in  $\mathbf{x}_6$  compared with the analytical one and, on the right, evolution of the approximated  $\tilde{u}_3$  at different heights along a vertical line in the center of the bar



The total wave field  $\mathbf{u}_{\text{tot}}$  is given by the sum of the incident wave  $\mathbf{u}_{\text{inc}}$  and the scattered one  $\mathbf{u}_{\text{sca}}$ , where the latter is reconstructed in a post-processing phase by using the single-layer representation formula (3.1), once the density  $\tilde{\mathbf{w}}$  is numerically computed. For the space discretization we choose a quasi-uniform mesh of  $\Gamma$  consisting of  $M_{\Delta_x} = 1488$ , with  $\Delta_x \simeq 0.125$ , while the time interval of interest is subdivided into  $N = 192$  subintervals so that  $c_P \simeq \frac{\Delta_x}{\Delta_t}$ . In this case, we have observed that  $N^* = 38$  and consequently the method is extremely fast.

In Figs. 13 and 14, we present several snapshots related to the components in the  $x_1$ - and  $x_2$ -directions, respectively, of the reconstructed scattered field in the square  $[-5, 5] \times [-5, 5]$ , laying on the plane  $x_3 = 0$  and external to the obstacle, for different time instants. We omit the plot of the component in the  $x_3$ -direction because it is trivial. These results show the capability of the proposed method to simulate a complete wavefield since an S-wave appears once the scattered field in  $x_1$ -direction, generated by the given Dirichlet datum, bumps against the obstacle and is reflected back.

862 **Conclusion and perspectives**

863 We have considered a boundary integral reformulation of 3D  
 864 time-domain interior and exterior wave problems, endowed

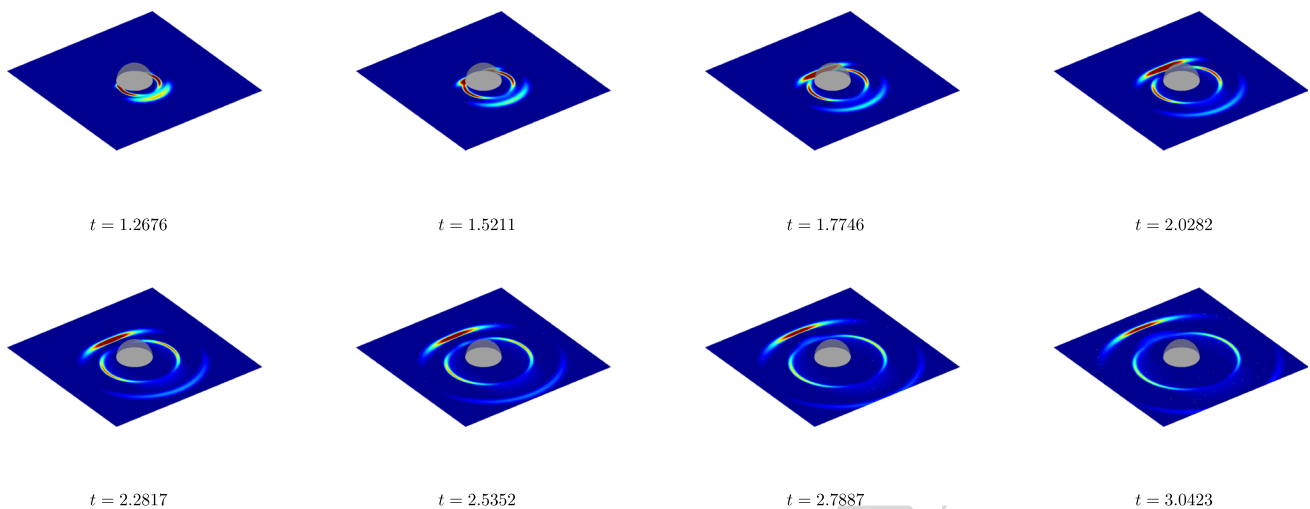


**Fig. 13** Scattering of a plane incident P-wave by the unit sphere. Snapshots of the component in the  $x_1$ -direction of the reconstructed scattered field  $\mathbf{u}_{sca}$  around the obstacle at different time instants

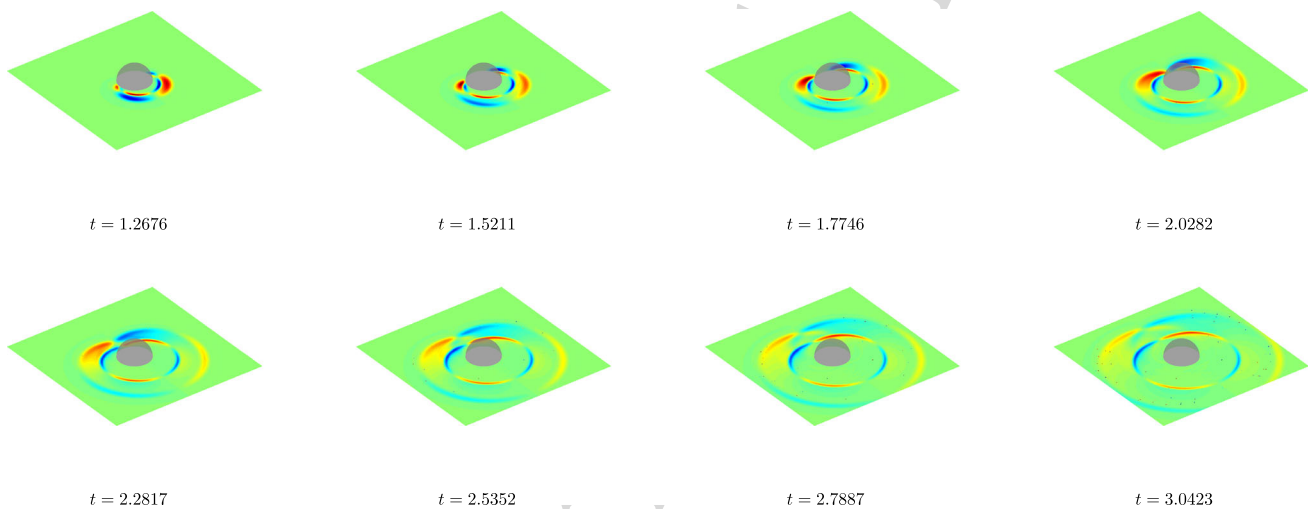


**Fig. 14** Scattering of a plane incident P-wave by the unit sphere. Snapshots of the component in the  $x_2$ -direction of the reconstructed scattered field  $\mathbf{u}_{sca}$  around the obstacle at different time instants

865 with a Dirichlet type boundary and null initial conditions.  
 866 For the resolution of the corresponding boundary integral  
 867 equation, we have used the space–time energetic Galerkin  
 868 boundary element method with double analytical integration  
 869 in time variable. The resulting weakly singular double integrals  
 870 in space variables are then evaluated by inner analytical  
 871 and outer numerical integrations. This issue has already been  
 872 encountered and analysed in [5], where the energetic BEM  
 873 has been applied to solve 3D acoustic (scalar) wave problems.  
 874 However, the extension of this method to the elastodynamic  
 875 (vector) case is not trivial, since a rigorous classification  
 876 of integration domains with shapes strongly dependent on  
 877 the advancement of P- and S-wave fronts is required. The  
 878 accurate detection of these domains is essential to avoid  
 879 computational inaccuracy and to overcome the difficulties

880 entailed by the integration of the Heaviside functions, that  
 881 model the wave fronts propagation. This issue, as already  
 882 observed in the context of 2D elastodynamic wave problems  
 883 (see [11]), is crucial to maintain the global efficiency and  
 884 stability of the entire energetic procedure. Furthermore, we  
 885 have theoretically and numerically shown that the compu-  
 886 tational cost and memory storage required by the proposed  
 887 numerical method can be significantly reduced by taking into  
 888 account a cut-off property known since the work of Mansur  
 889 [28] and used for instance in [25, 26].

890 Unfortunately, even if the energetic BEM takes advantage  
 891 from the dimensionality reduction of the problem, working  
 892 on the boundary and not on the spatial domain, 3D realistic  
 893 problems involve a large number of surface degrees of  
 894 freedom. Therefore, the traditional implementation on ordi-

895 nary laptops of the method is prohibitive as soon as the space  
 896 dimension becomes large, and it is restricted to problems of  
 897 small size, typically  $\mathcal{O}(10^3)$  degrees of freedom, as shown  
 898 in the presented numerical tests. We remark that at the cur-  
 899 rent stage the design and the implementation of fast, stable  
 900 and accurate solvers, that allow to increase the capabilities of  
 901 space–time BEMs, are still open questions (see [12] and [20]  
 902 for recent developments in 2D). Even if this issue is crucial  
 903 for successful applications of the proposed method to large  
 904 scale HPC applications, it is out of the aim of the present pio-  
 905 neering paper. Since these aspects are worth of study, they  
 906 will be the subject of future investigations. On the other side,  
 907 the study of Energetic BEM for the more interesting 3D elas-  
 908 todynamic PDE equipped by mixed or Neumann boundary  
 909 condition is currently taken into account, with the develop-  
 910 ment of space–time double layer potential and hypersingular  
 911 integral operator discretizations, extending what has been  
 912 done in [6] for 3D acoustic wave propagation.

### 913 Appendix

914 In the case of acoustic (scalar) wave propagation problems,  
 915 for a given child triangle  $\check{E}_m^{(k)}$  a single circular wave front  
 916 induces, in the most general case, a partition represented by  
 917 (the sum of) a triangle (region  $\mathcal{G}$ ) and two circular sectors  
 918 (region  $\mathcal{E}$ ). In this Appendix, we detail the analytical inner  
 919 integration over these two types of domain.

### 920 A Results of the analytical integration over a 921 circular sector

922 We have already remarked that, when  $\rho_\blacklozenge = 0$ , the domain  
 923  $\mathcal{F}$  coincides with  $\mathcal{E}$  (circular sector). In this special case, the  
 924 expression of the functions  $K_{i,j}(\rho_\blacklozenge) := K_{i,j}(0, \rho_\blacklozenge)$ , for  
 925  $i = j = 1$  or  $i = 1, 2, 3$  and  $j = 3, 5$ , simplifies as it  
 926 follows:

$$927 \quad K_{1,1}(\rho_\blacklozenge) := \sqrt{\rho_\blacklozenge^2 + z^2} - z$$

$$928 \quad K_{1,3}(\rho_\blacklozenge) := -\frac{1}{\sqrt{\rho_\blacklozenge^2 + z^2}} + \frac{1}{z}$$

$$929 \quad K_{1,5}(\rho_\blacklozenge) := \frac{1}{3} \left[ \frac{1}{z^3} - \left( \frac{1}{\sqrt{\rho_\blacklozenge^2 + z^2}} \right)^3 \right]$$

$$930 \quad K_{2,3}(\rho_\blacklozenge) := \log \left( \frac{\rho_\blacklozenge + \sqrt{\rho_\blacklozenge^2 + z^2}}{z} \right) - \frac{\rho_\blacklozenge}{\sqrt{\rho_\blacklozenge^2 + z^2}}$$

$$931 \quad K_{2,5}(\rho_\blacklozenge) := \frac{1}{3z^2} \left( \frac{\rho_\blacklozenge}{\sqrt{\rho_\blacklozenge^2 + z^2}} \right)^3$$

$$932 \quad K_{3,3}(\rho_\blacklozenge) := \sqrt{\rho_\blacklozenge^2 + z^2} + \frac{z^2}{\sqrt{\rho_\blacklozenge^2 + z^2}} - 2z$$

$$933 \quad K_{3,5}(\rho_\blacklozenge) := \frac{2}{3z} - \frac{1}{\sqrt{\rho_\blacklozenge^2 + z^2}} + \frac{z^2}{3} \left( \frac{1}{\sqrt{\rho_\blacklozenge^2 + z^2}} \right)^3.$$

934 Since they depend on  $z$ , we point out that in this scenario  $z$   
 935 is always greater than 0.

### 936 B Results of the analytical integration over a 937 triangle

938 For what concerns the collapsed version of the domain  $\mathcal{H}$ , i.e.  
 939 the triangle  $\mathcal{G}$ , we report here the values of  $\tilde{K}_{i,j}^{h,k}(\theta_\blacklozenge, \theta_\blackheartsuit) :=$   
 940  $\tilde{K}_{i,j}^{h,k}(0; \theta_\blacklozenge, \theta_\blackheartsuit)$ , where the indices  $h, k = 1, 2, 3$  are such  
 941 that  $2 \leq h + k < 5$ , while the indices  $i$  and  $j$  are such that  
 942  $i = j = 1$  or  $i = 1, 2, 3$  and  $j = 3, 5$ . For easiness of the  
 943 presentation, we collect the expression of  $\tilde{K}_{i,j}^{h,k}(\theta_\blacklozenge, \theta_\blackheartsuit)$  on  
 944 the basis of the values of the indices  $h$  and  $k$ , so that

- 945 • for  $h = k = 1$  we have:

$$946 \quad \tilde{K}_{1,1}^{1,1}(\theta_\blacklozenge, \theta_\blackheartsuit) := Fg_3(\theta_\blacklozenge, \theta_\blackheartsuit) + zg_6(\theta_\blacklozenge, \theta_\blackheartsuit)$$

$$947 \quad - z(\theta_\blackheartsuit - \theta_\blacklozenge)$$

$$948 \quad \tilde{K}_{1,3}^{1,1}(\theta_\blacklozenge, \theta_\blackheartsuit) := -\frac{1}{z}g_6(\theta_\blacklozenge, \theta_\blackheartsuit) + \frac{1}{z}(\theta_\blackheartsuit - \theta_\blacklozenge)$$

$$949 \quad \tilde{K}_{1,5}^{1,1}(\theta_\blacklozenge, \theta_\blackheartsuit) := -\frac{1}{3z^2} \frac{F}{F^2 + z^2}$$

$$950 \quad \left[ \frac{\cos(\theta_\blackheartsuit + \beta)}{g_2(\theta_\blacklozenge, \theta_\blackheartsuit)} - \frac{\cos(\theta_\blacklozenge + \beta)}{g_1(\theta_\blacklozenge, \theta_\blackheartsuit)} \right]$$

$$951 \quad - \frac{g_6(\theta_\blacklozenge, \theta_\blackheartsuit)}{3z^3} + \frac{\theta_\blackheartsuit - \theta_\blacklozenge}{3z^3}$$

- 952 • for  $h = 1$  and  $k = 2$  we have

$$953 \quad \tilde{K}_{2,3}^{1,2}(\theta_\blacklozenge, \theta_\blackheartsuit) := g_5(\theta_\blacklozenge, \theta_\blackheartsuit) \cos(\gamma - \theta_\blackheartsuit) - g_4(\theta_\blacklozenge, \theta_\blackheartsuit)$$

$$954 \quad \cos(\gamma - \theta_\blacklozenge) - g_3(\theta_\blacklozenge, \theta_\blackheartsuit) \cos \alpha$$

$$955 \quad \tilde{K}_{2,5}^{1,2}(\theta_\blacklozenge, \theta_\blackheartsuit) := \frac{1}{3z^2}$$

$$956 \quad \times \left[ \frac{\sin \alpha \sin(\theta_\blackheartsuit + \beta) - g_7(\theta_\blacklozenge, \theta_\blackheartsuit) \cos \alpha \cos(\theta_\blackheartsuit + \beta)}{g_2(\theta_\blacklozenge, \theta_\blackheartsuit)} + \right.$$

$$957 \quad \left. + \frac{g_7(\theta_\blacklozenge, \theta_\blackheartsuit) \cos \alpha \cos(\theta_\blacklozenge + \beta) - \sin \alpha \sin(\theta_\blacklozenge + \beta)}{g_1(\theta_\blacklozenge, \theta_\blackheartsuit)} \right]$$

- 958 • for  $h = 1$  and  $k = 3$  we have

$$\begin{aligned}
 \tilde{K}_{3,3}^{1,3}(\theta_\diamond, \theta_\heartsuit) &:= F[g_2(\theta_\diamond, \theta_\heartsuit) \cos(\theta_\heartsuit + \alpha - \gamma) \\
 &\quad - g_1(\theta_\diamond, \theta_\heartsuit) \cos(\theta_\diamond + \alpha - \gamma) + g_3(\theta_\diamond, \theta_\heartsuit) \sin^2 \alpha] \\
 &\quad + zg_6(\theta_\diamond, \theta_\heartsuit) - 2z\Theta_{1,3}(\theta_\diamond, \theta_\heartsuit) \\
 \tilde{K}_{3,5}^{1,3}(\theta_\diamond, \theta_\heartsuit) &:= \frac{2}{3z}\Theta_{1,3}(\theta_\diamond, \theta_\heartsuit) - \frac{g_6(\theta_\diamond, \theta_\heartsuit)}{3z} \\
 &\quad + \frac{g_7(\theta_\diamond, \theta_\heartsuit) \cos^2 \alpha \cos(\theta_\heartsuit + \beta) - \cos(\theta_\heartsuit + \alpha - \gamma) \sin^2(\theta_\heartsuit + \beta)}{3Fg_2(\theta_\diamond, \theta_\heartsuit)} \\
 &\quad - \frac{g_7(\theta_\diamond, \theta_\heartsuit) \cos^2 \alpha \cos(\theta_\diamond + \beta) - \cos(\theta_\diamond + \alpha - \gamma) \sin^2(\theta_\diamond + \beta)}{3Fg_1(\theta_\diamond, \theta_\heartsuit)}
 \end{aligned}$$

- 965 • for  $h = 2$  and  $k = 1$  we have

$$\begin{aligned}
 \tilde{K}_{2,3}^{2,1}(\theta_\diamond, \theta_\heartsuit) &:= -g_5(\theta_\diamond, \theta_\heartsuit) \cos \theta_\heartsuit + g_4(\theta_\diamond, \theta_\heartsuit) \cos \theta_\diamond \\
 &\quad - g_3(\theta_\diamond, \theta_\heartsuit) \cos \beta \tilde{K}_{2,5}^{2,1}(\theta_\diamond, \theta_\heartsuit) := \frac{1}{3z^2} \\
 &\quad \times \left[ \frac{\sin \beta \sin(\theta_\diamond + \beta) + g_7(\theta_\diamond, \theta_\heartsuit) \cos \beta \cos(\theta_\diamond + \beta)}{g_1(\theta_\diamond, \theta_\heartsuit)} + \right. \\
 &\quad \left. - \frac{\sin \beta \sin(\theta_\heartsuit + \beta) + g_7(\theta_\diamond, \theta_\heartsuit) \cos \beta \cos(\theta_\heartsuit + \beta)}{g_2(\theta_\diamond, \theta_\heartsuit)} \right]
 \end{aligned}$$

- 970 • for  $h = k = 2$  we have

$$\begin{aligned}
 \tilde{K}_{3,3}^{2,2}(\theta_\diamond, \theta_\heartsuit) &:= F[g_1(\theta_\diamond, \theta_\heartsuit) \cos(\theta_\diamond + \alpha) \\
 &\quad - g_2(\theta_\diamond, \theta_\heartsuit) \cos(\theta_\heartsuit + \alpha) - g_3(\theta_\diamond, \theta_\heartsuit) \sin \alpha \sin \beta] \\
 &\quad - zg_6(\theta_\diamond, \theta_\heartsuit) \cos \gamma - 2z\Theta_{2,2}(\theta_\diamond, \theta_\heartsuit)
 \end{aligned}$$

- 974 • for  $h = 3$  and  $k = 1$  we have

$$\begin{aligned}
 \tilde{K}_{3,3}^{3,1}(\theta_\diamond, \theta_\heartsuit) &:= F[g_1(\theta_\diamond, \theta_\heartsuit) \cos(\theta_\diamond - \beta) \\
 &\quad - g_2(\theta_\diamond, \theta_\heartsuit) \cos(\theta_\heartsuit - \beta) + g_3(\theta_\diamond, \theta_\heartsuit) \sin^2 \beta] \\
 &\quad + zg_6(\theta_\diamond, \theta_\heartsuit) - 2z\Theta_{3,1}(\theta_\diamond, \theta_\heartsuit).
 \end{aligned}$$

978 Even in this case,  $z$  is always greater than 0.

## 979 References

- 980 1. Abramowitz M, Stegun I (1964) Handbook of mathematical functions. NBS (1964)
- 981 2. Aimi A, Diligenti M (2008) A new space–time energetic formulation for wave propagation analysis in layered media by BEMs. *Int J Numer Methods Eng* 75(9):1102–1132
- 982 3. Aimi A, Diligenti M, Guardasoni C, Mazziari I, Panizzi S (2009) An energy approach to space–time Galerkin BEM for wave propagation problems. *Int J Numer Methods Eng* 80(9):1196–1240
- 983 4. Aimi A, Diligenti M, Frangi A, Guardasoni C (2012) A stable 3D energetic Galerkin BEM approach for wave propagation interior problems. *Eng Anal Bound Elem* 36(12):1756–1765
- 984 5. Aimi A, Diligenti M, Frangi A, Guardasoni C (2013) Neumann exterior wave propagation problems: computational aspects of 3D energetic Galerkin BEM. *Comput Mech* 51(4):475–493
- 985 6. Aimi A, Diligenti M, Frangi A, Guardasoni C (2014) Energetic BEM-FEM coupling for wave propagation in 3D multidomains. *Int J Numer Method Eng* 97:377–394
- 986 7. Aimi A, Desiderio L, Diligenti M, Guardasoni C (2014) A numerical study of energetic BEM-FEM applied to wave propagation in 2D multidomains. *Publications de l’Institut Mathématique* 96(110):5–22
- 987 8. Aimi A, Desiderio L, Diligenti M, Guardasoni C (2019) Application of energetic BEM to 2D elastodynamic soft scattering problems. *Commun Appl Ind Math* 10(1):182–198
- 988 9. Aimi A, Desiderio L, Fedeli P, Frangi A (2021) A fast boundary-finite element approach for estimating anchor losses in micro-electro-mechanical system resonators. *Appl Math Model* 97:741–753
- 989 10. Aimi A, Di Credico G, Gimperlein H, Stephan EP. Higher-order time domain boundary elements for elastodynamics—graded meshes and hp-versions (under review)
- 990 11. Aimi A, Di Credico G, Diligenti M, Guardasoni C (2022) Highly accurate quadrature schemes for singular integrals in energetic BEM applied to elastodynamics. *J Comput Appl Math* 410:114186
- 991 12. Aimi A, Desiderio L, Di Credico G (2022) Partially pivoted ACA based acceleration of the Energetic BEM for time-domain acoustic and elastic waves exterior problems. *Comput Math Appl* 119:351–370
- 992 13. Anderson TG, Bruno OP, Lyon M (2020) High-order, dispersionless “fast-hybrid” wave equation solver. Part I: O(1) sampling cost via incident-field windowing and recentering. *SIAM J Sci Comput* 42(2):A1348–A1379
- 993 14. Bamberger A, Ha Duong T (1986) Formulation variationnelle espace-temps pour le calcul par potentiel retardé de la diffraction d’une onde acoustique. *Math Methods Appl Sci* 8:405–435
- 994 15. Bonnet M (1995) Boundary integral equation methods for solids and fluids. Wiley, Hoboken
- 995 16. Chaillat S, Desiderio L, Ciarlet P Jr (2017) Theory and implementation of  $\mathcal{H}$ -matrix based iterative and direct solvers for oscillatory kernels. *J Comput Phys* 351:165–186
- 996 17. Chen G, Zhou J (2010) Boundary element methods with applications to nonlinear problems. Atlantis Press, Paris
- 997 18. Costabel M (2004) Time-dependent problems with the boundary integral equation method. *Encycl Comput Mech* 1:703–721
- 998 19. Desiderio L (1978) An  $\mathcal{H}$ -matrix based direct solver for the Boundary Element Method in 3D elastodynamics. *AIP Conf Proc* 2018:120005
- 999 20. Desiderio L, Falletta S (2020) Efficient solution of two-dimensional wave propagation problems by CQ-wavelet BEM: algorithm and applications. *SIAM J Sci Comput* 42(4):B894–B920
- 1000 21. Eringen AC, Suhubi ES (1975) *Elastodynamics*. Academic Press, New York
- 1001 22. Geuzaine C, Remacle JF (2009) Gmsh: a three-dimensional finite element mesh generator with built-in pre- and post processing facilities. *Int J Numer Methods Eng* 79:1309–1331
- 1002 23. Jang HW, Ih JG (2012) Stabilization of time domain acoustic boundary element method for the exterior problem avoiding the nonuniqueness. *J Acoust Soc Am* 133(3):1237–1244
- 1003 24. Joly P, Rodriguez J (2017) Mathematical aspects of variational boundary integral equations for time dependent wave propagation. *J Integr Equ Appl* 29(1):137–187
- 1004 25. Kager B (2014) Efficient convolution quadrature based boundary element formulation for time-domain elastodynamics. PhD Thesis, Technischen Universität Graz
- 1005 26. Kager B, Schanz M (2015) Fast and data sparse time domain BEM for elastodynamics. *Eng Anal Bound Elem* 50:212–223
- 1006 27. Lubich C (1994) On the multistep time discretization of linear initial-boundary value problems and their boundary integral equations. *Numer Math* 67(3):365–389

- 1059 28. Mansur WJ (1983) A time-stepping technique to solve wave prop- 1076  
1060 agation problems using the boundary element method. PhD thesis, 1077  
1061 University of Southampton  
1062 29. Mansur WJ, Brebbia CA (1985) Further developments on the solu- 1078  
1063 tion of the transient scalar wave equation. In: Brebbia CA (ed) 1079  
1064 Topics in boundary elements research 2. Springer, Berlin, pp 87–  
1065 123  
1066 30. Martin PA (2021) Time-domain scattering. Cambridge University  
1067 Press, Cambridge  
1068 31. Milroy J, Hinduja S, Davey K (1997) The elastostatic three-  
1069 dimensional boundary element method: analytical integration  
1070 for linear isoparametric triangular elements. Appl Math Model  
1071 21:763–782  
1072 32. Norwood FR (1967) Diffraction of transient elastic waves by a  
1073 spherical cavity. Ph.D. Thesis, Caltech  
1074 33. Quarteroni A, Valli A (1994) A numerical approximation of partial  
1075 differential equations. Springer, Berlin
34. Rynne BP (1985) Stability and convergence of time marching  
methods in scattering problems. IMA J Appl Math 35(3):297–310  
35. Schanz M (2018) Fast multipole method for poroelastodynamics.  
Eng Anal Bound Elem 89:50–59

**Publisher's Note** Springer Nature remains neutral with regard to juris- 1080  
dictional claims in published maps and institutional affiliations. 1081

Springer Nature or its licensor (e.g. a society or other partner) holds  
exclusive rights to this article under a publishing agreement with the  
author(s) or other rightsholder(s); author self-archiving of the accepted  
manuscript version of this article is solely governed by the terms of such  
publishing agreement and applicable law.

Uncorrected proof

## Author Query Form

**Please ensure you fill out your response to the queries raised below  
and return this form along with your corrections**

Dear Author

During the process of typesetting your article, the following queries have arisen. Please check your typeset proof carefully against the queries listed below and mark the necessary changes either directly on the proof/online grid or in the 'Author's response' area provided below

<b>Query</b>	<b>Details required</b>	<b>Author's response</b>
1.	Please check and confirm the edit made in the article title.	
2.	Please check and confirm the inserted city for the affiliations 1 and 2.	
3.	Please provide the complete details for the reference Aimi et al. (under review).	